




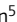







## ARTICLE

# Modulating the quantity of HIV Env-specific CD4 T cell help promotes rare B cell responses in germinal centers

Jeong Hyun Lee<sup>1,2</sup> , Joyce K. Hu<sup>1</sup> , Erik Georgeson<sup>2,3,4</sup> , Catherine Nakao<sup>1</sup> , Bettina Groschel<sup>2,3,4</sup> , Thamotharampillai Dileepan<sup>5</sup> , Marc K. Jenkins<sup>5</sup> , Gregory Seumois<sup>1</sup> , Pandurangan Vijayanand<sup>1,6</sup> , William R. Schief<sup>2,3,4,7</sup> , and Shane Crotty<sup>1,2,8</sup> 

**Immunodominance to nonneutralizing epitopes is a roadblock in designing vaccines against several diseases of high interest. One hypothetical possibility is that limited CD4 T cell help to B cells in a normal germinal center (GC) response results in selective recruitment of abundant, immunodominant B cells. This is a central issue in HIV envelope glycoprotein (Env) vaccine designs, because precursors to broadly neutralizing epitopes are rare. Here, we sought to elucidate whether modulating the quantity of T cell help can influence recruitment and competition of broadly neutralizing antibody precursor B cells at a physiological precursor frequency in response to Env trimer immunization. To do so, two new Env-specific CD4 transgenic (Tg) T cell receptor (TCR) mouse lines were generated, carrying TCR pairs derived from Env-protein immunization. Our results suggest that CD4 T cell help quantitatively regulates early recruitment of rare B cells to GCs.**

## Introduction

A key aspect of the humoral immune response is antibodies arising as a result of cellular compartments called germinal centers (GCs), where B cells capable of recognizing the invading pathogen undergo somatic hypermutation to eventually produce high-affinity antibodies (Mesin et al., 2016). Because the maturation of high-affinity B cells is an evolutionary process, factors that affect the evolutionary fitness of GC B cells ( $B_{GC}$ ) influence the outcome of the immune response. Another fundamental player in the GC response is the T follicular helper ( $T_{FH}$ ) cell (Crotty, 2019).  $T_{FH}$  cells are required to recruit B cells into the GC and drive selection of high-affinity B cells as they undergo mutation in the GC. These interactions lead to the generation of protective responses against many pathogens, but ironically the evolutionarily competitive nature of the response can result in failure to elicit robust neutralizing antibodies (nAbs) against certain types of antigens. For example, B cell immunodominance can influence the outcome of the humoral response and is often observed in B cell responses to HIV-1 envelope glycoprotein (Env) or influenza hemagglutinin (Havenar-Daughton et al., 2017; Angeletti and Yewdell, 2018). These viruses have high

sequence diversity. While cross-strain responses are attainable, they are uncommon because immunodominance highly favors easily accessible epitopes that are not well conserved between different viral isolates. Furthermore, although  $T_{FH}$  cells are central to the GC response, it is unknown how increasing help from  $T_{FH}$  cells influences immunodominance. Would increasing accessibility to T cell help preferentially enhance the uncommon but desired B cell responses? Or, equally probable, would increasing early T cell help fuel B cell immunodominance even further?

Immunodominance is a major roadblock to HIV vaccine discovery. Env, a trimeric glycoprotein consisting of non-covalently assembled glycoprotein (gp) 120 and gp41 subunits, is the sole surface antigen on HIV, but it has an extremely high sequence diversity among circulating strains and is heavily glycosylated, blocking accessibility to much of its conserved immunogenic protein surface. One immune evasion mechanism that the virus uses is shedding of gp120 monomers and displaying other nonfunctional conformations of the Env protein, which reveal proteinaceous neoepitopes that are not present on

<sup>1</sup>Center for Infectious Disease and Vaccine Research, La Jolla Institute for Immunology, La Jolla, CA; <sup>2</sup>Consortium for HIV/AIDS Vaccine Development, The Scripps Research Institute, La Jolla, CA; <sup>3</sup>International AIDS Vaccine Initiative Neutralizing Antibody Center, The Scripps Research Institute, La Jolla, CA; <sup>4</sup>Department of Immunology and Microbiology, The Scripps Research Institute, La Jolla, CA; <sup>5</sup>Department of Microbiology and Immunology, Center for Immunology, University of Minnesota Medical School, Minneapolis, MN; <sup>6</sup>Clinical and Experimental Sciences, National Institute for Health Research Southampton, Respiratory Biomedical Research Unit, University of Southampton, Southampton, UK; <sup>7</sup>Ragon Institute of Massachusetts General Hospital, Massachusetts Institute of Technology and Harvard University, Cambridge, MA; <sup>8</sup>Department of Medicine, Division of Infectious Diseases and Global Public Health, University of California, San Diego, La Jolla, CA.

Correspondence to Shane Crotty: [shane@lji.org](mailto:shane@lji.org).

© 2020 Lee et al. This article is distributed under the terms of an Attribution–Noncommercial–Share Alike–No Mirror Sites license for the first six months after the publication date (see <http://www.rupress.org/terms/>). After six months it is available under a Creative Commons License (Attribution–Noncommercial–Share Alike 4.0 International license, as described at <https://creativecommons.org/licenses/by-nc-sa/4.0/>).

the functional viral spike (Burton and Mascola, 2015). This results in much of the initial response to HIV (or simian immunodeficiency virus [SIV]) infection eliciting nonneutralizing antibodies. Even with the advent of stabilized, native-like soluble Env trimer immunogens such as the BG505 SOSIP trimer (Sanders et al., 2013), the most accessible epitopes tend to be in regions where glycans are missing owing to strain-specific deficiency of an N-linked glycosylation site (McCoy et al., 2016; Crooks et al., 2017; Wagh et al., 2018; Ringe et al., 2019; Klasse et al., 2018). Also, in soluble Env trimer immunogen vaccination studies, the base of the trimer (which is devoid of glycans but is unexposed on viruses and therefore is a nonneutralizing site) is routinely identified to be immunodominant (Cirelli et al., 2019; Hu et al., 2015; McCoy et al., 2016; Bianchi et al., 2018). In natural infections, ~10–50% of chronically infected HIV<sup>+</sup> patients develop broadly neutralizing antibodies (bnAbs) that target conserved but immunosilent epitopes that are heavily surrounded by glycans, by directly binding or sterically circumventing highly conserved N-linked glycans on Env (Burton and Hangartner, 2016). However, naive precursor B cells that have the capacity to evolve into bnAbs are rare (Jardine et al., 2016; Havenar-Daughton et al., 2018; Steichen et al., 2019), emphasizing the difficulty in recruiting the correct B cells to the GC in lieu of the immunodominant B cells.

In Env immunization studies in nonhuman primates (NHPs), increased B<sub>GC</sub> cells and nAbs were correlated with antigen-specific T<sub>FH</sub> cells (Cirelli et al., 2019; Pauthner et al., 2017; Havenar-Daughton et al., 2016a). Likewise, in HIV infection, the development of bnAbs was correlated with higher frequencies of circulating T<sub>FH</sub> cells (Locci et al., 2013; Yamamoto et al., 2015; Moody et al., 2016). Acquisition of help from T<sub>FH</sub> cells is dependent on the ability of antigen-specific B cells to process and present cognate T cell epitopes via their MHC class II molecules. Yet it is conceivable that the majority of the Env protein sequence space cannot be used for MHC class II presentation due to the heavily glycosylated nature of Env. For example, in C57BL/6 mice, MHC class II responses to two different Envs were limited to approximately five distinct regions of the Env protein (Surman et al., 2001; Brown et al., 2003), and among live-attenuated SIV immunized rhesus macaques, SIV Env ectodomain-directed MHC class II responses were largely restricted to unglycosylated regions (Sarkar et al., 2002). In another study, serum responses to core gp120 molecules in small-animal models were limited and could be boosted by the addition of the universal T-helper epitope, pan-DR-helper epitope, to the termini of the same gp120 construct (Grundner et al., 2004). Thus, restricted CD4 T cell epitopes combined with low precursor frequency of bnAb class B cells suggest that access to T<sub>FH</sub> help may be an additional conundrum in the elicitation of potent bnAb responses (Havenar-Daughton et al., 2017; Klasse et al., 2020).

These previous studies highlight that a thorough understanding of how T cell help to B cells in an immunodominant setting would be informative for identifying factors that predict successful protective immune responses. However, there has been a lack of experimental models available to investigate the effect of T cell help on rare B cells in response to an immunologically difficult antigen such as Env. We established two new

Env-specific transgenic (Tg) TCR mouse lines that harbor TCR sequences from authentic Env-specific murine T<sub>FH</sub> cells. By combining our newly created Tg TCR CD4 T cells with a physiological bnAb precursor B cell mouse model (Abbott et al., 2018), we present a new approach for studying the impact of T cells in the context of a difficult antigen.

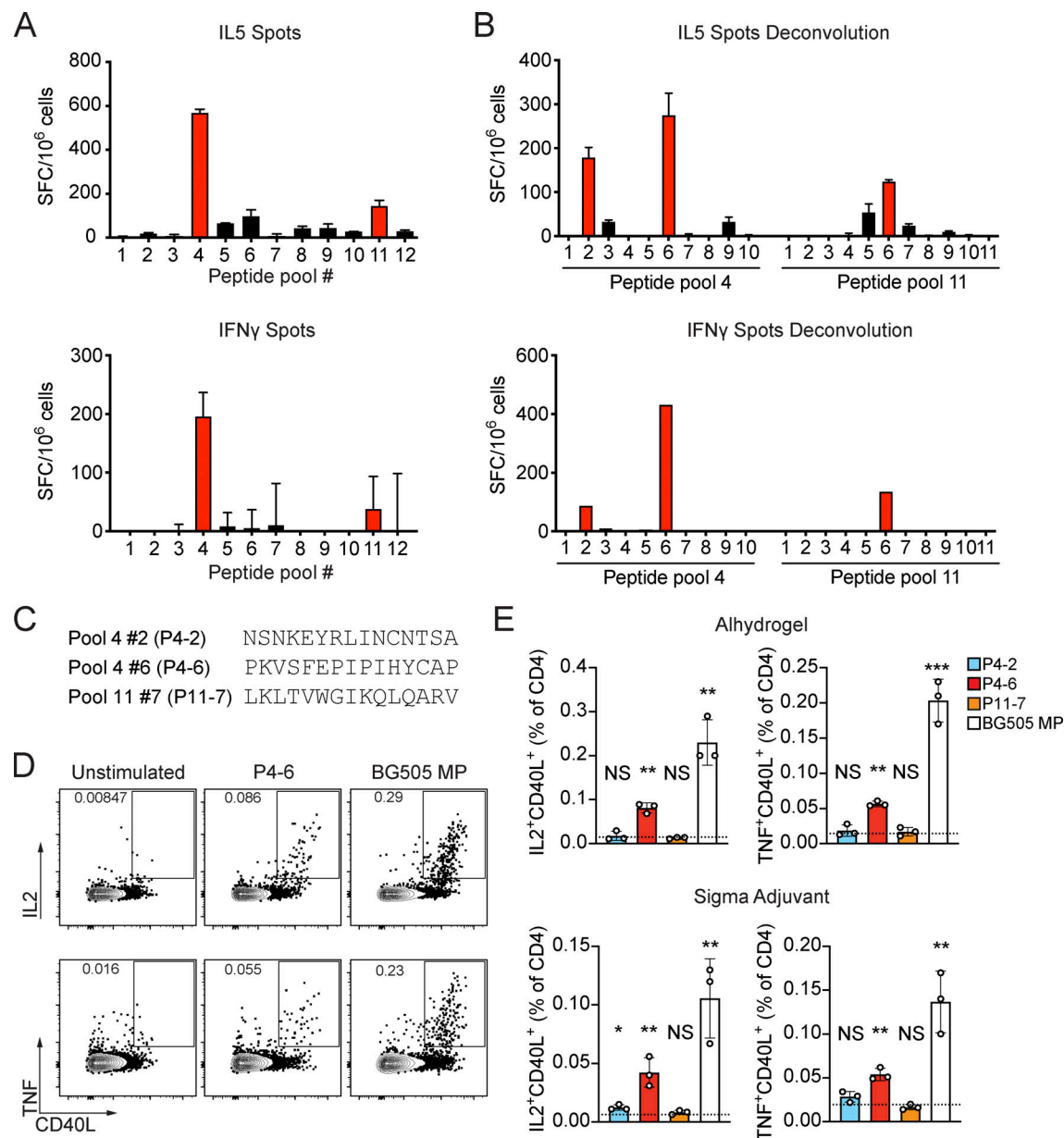
## Results

### Identification of Env-specific MHC class II epitopes in mice

The Env trimer is highly glycosylated, and therefore peptide processing and presentation by antigen-presenting cells (APCs) may be hampered by glycans flanking, or within, MHC class II epitopes. Conjugating a known non-HIV MHC class II epitope to the N- or C-terminus of the Env protein may not reflect how natural Env-derived T cell epitopes are processed and presented by APCs, and would likely be subject to proteolytic digestion. We sought to develop an Env-specific Tg TCR mouse representing a relatively normal CD4 T cell response to a native-like Env trimer, dependent on natural proteolytic peptide processing and presentation by APCs. To this end, instead of a classic peptide immunization and hybridoma approach to identify TCRs, we proceeded to directly sequence Env-specific TCRs after immunizing C57BL/6 mice with the soluble Env protein.

First, we identified I-A<sup>d</sup>/I-E<sup>d</sup> restricted epitopes, as a follow-up to a BG505 SOSIP trimer immunization study in Balb/c mice (Hu et al., 2015). Mice received s.c. immunizations with BG505 SOSIP trimer at weeks 0 and 3. At week 4, the CD4 T cells from spleens and draining LNs were restimulated *ex vivo* with overlapping BG505 Env 15-mer peptides divided into 12 pools. BG505-specific IL5- and IFN $\gamma$ -producing CD4 T cells were identified, with responses directed to pool 4 (in gp120) and pool 11 (in gp41; Fig. 1 A). Deconvolution of the peptide pools revealed three I-A<sup>d</sup> epitopes: P4-2 (NSNKEYRLINCNTSA) in gp120 variable region 2 (V2); P4-6 (PKVSFEPIPIHYCAP) in gp120 constant region 2 (C2); and P11-6 (LKLTVWGKQLQARV) in gp41 heptad repeat 1, with the greatest response being toward P4-6 (Fig. 1, B and C).

We also mapped I-A<sup>b</sup> restricted epitopes in BG505 SOSIP, because generating a Tg TCR mouse on C57BL/6 background would allow us to set up a T and B cell cotransfer model with Tg B cell receptor (BCR) mice expressing various germline reverted bnAb BCRs (Dosenovic et al., 2015; Escolano et al., 2016; Tian et al., 2016; Williams et al., 2017; Abbott et al., 2018; Steichen et al., 2019). After i.p. immunizing C57BL/6 mice with soluble BG505 Env mixed with Alhydrogel alum or Sigma adjuvant, splenocytes isolated 8–10 d after immunization were *ex vivo* restimulated with the three 15-mer peptides that were found to be immunodominant in Balb/c mice (Fig. 1 C), along with a complete BG505 Env peptide megapool (MP) containing overlapping 15-mer peptides covering the full sequence of Env. Intracellular cytokine staining (ICS) was performed to quantify IL2- and TNF-producing CD4 T cells. Env peptide P4-6 was found to comprise ~25% of the BG505-directed CD4 T cell response in C57BL/6 mice (Fig. 1, D and E). This was in agreement with a previous publication in which the conserved C2 region surrounding P4-6 was identified as an immunodominant MHC



**Figure 1. Env-specific MHC class II epitope mapping after Env trimer immunization. (A and B)** Balb/c mice immunized s.c. with BG505 trimer in Abisco-100 adjuvant at 0 and 3 wk were sacrificed at 4 wk. ELISPOT was performed after overnight stimulation (20 h) of combined CD4 T cells from spleen, inguinal, and popliteal LNs with 10  $\mu$ g/ml of peptide pools ( $\sim$ 1  $\mu$ g/ml per peptide) or 1  $\mu$ g/ml of each peptide for the deconvolution. Mean and SD are shown.  $N = 2$ ,  $n = 3$ , where  $N$  corresponds to number of independent experiments and  $n$  represents the number of mice per group in a given experiment. A representative experiment is shown. **(A)** Spot-forming cells (SFCs) producing IL5 (upper) or IFN $\gamma$  (lower) following stimulation with indicated peptide pools. **(B)** SFCs producing IL5 (upper) or IFN $\gamma$  (lower) following stimulation with individual peptides within peptide pools 4 and 11. **(C)** Sequences of 15-mer peptides identified by deconvolution in B. **(D and E)** C57BL/6 mice immunized i.p. with the BG505 MP or 5  $\mu$ g/ml of each of the peptides listed in C.  $N = 2$ ,  $n = 3$ . A representative experiment is shown. **(D)** Representative flow plots from an alum-immunized mouse. Gated on CD4<sup>+</sup>/CD44<sup>+</sup>CD62L<sup>+</sup> activated CD4 T cells. Frequencies shown for the cytokine gates are percentage cytokine-positive of CD4 T cells. **(E)** Quantification of IL2<sup>+</sup>CD40L<sup>+</sup> and TNF<sup>+</sup>CD40L<sup>+</sup> CD4 T cells following stimulation with indicated peptides. Dotted lines indicate average background signal from the unstimulated condition. Mean and SD are shown. Statistics denote pairwise comparison between the unstimulated condition and each of the peptides tested. NS,  $> 0.05$ ; \*,  $P \leq 0.05$ ; \*\*,  $P \leq 0.01$ ; \*\*\*,  $P \leq 0.001$  (unpaired two-tailed Student's  $t$  test).

class II epitope in C57BL/6 mice immunized with nontrimeric Envs from a clade B isolate, 1007, and a clade D isolate, UG92005 (Surman et al., 2001). Notably, the Env P4-6 epitope identified here in Balb/c and C57BL/6 mice was also observed to be an immunodominant CD4 T cell epitope in Env among HIV-infected humans (Ranasinghe et al., 2012).

#### Generation of Env-specific CD4 Tg TCR mice

We selected Env P4-6 (hereon referred to as HYCAP-p15: PKVSFEPIPIHYCAP) and proceeded to identify TCR sequences from HYCAP-p15-specific T<sub>H</sub> cells. ICS is not ideal for detecting antigen-specific T<sub>H</sub> cells, because T<sub>H</sub> cells generally produce small quantities of cytokines (Dan et al., 2016; Havenar-Daughton

et al., 2016b). The fixation process required to permeabilize cells for ICS is also highly damaging to mRNA. Our laboratory has previously demonstrated that cytokine-independent activation-induced markers (AIM) are better suited for identifying antigen-specific human and NHP  $T_{FH}$  cells (Dan et al., 2016; Havenar-Daughton et al., 2016b; Reiss et al., 2017). Therefore, to develop an AIM assay for murine  $T_{FH}$  cells, we tested CD40L and CD69 as candidate surface markers to detect known antigen-specific CD4 T cells, by adoptively transferring SMARTA CD4 T cells (lymphocytic choriomeningitis virus [LCMV] gp<sub>66-77</sub>, I-A<sup>b</sup> restricted) followed by immunization with LCMV gp<sub>61-80</sub> peptide conjugated to a carrier protein, KLH (KLH-gp<sub>61</sub>). Upon ex vivo restimulation with gp<sub>66-77</sub> peptide, ~72% of SMARTA CD4 T cells and SMARTA  $T_{FH}$  cells were identified as CD40L<sup>+</sup>CD69<sup>+</sup> (9 h; Fig. 2, A and B). We next immunized C57BL/6 mice with BG505 Env trimer and stained cells for CD40L and CD69, along with CD25 and OX40 as additional potential AIM markers (Fig. S1, A and B), as they work well in human and NHP AIM assays (Dan et al., 2016; Havenar-Daughton et al., 2016b). However, upon restimulation with the HYCAP-p15 peptide, murine CD4 T cells expressing either CD25 or OX40 were predominantly CD40L<sup>+</sup> and Foxp3<sup>+</sup> regulatory T cells (Fig. S1, A and C), as expected because of the high CD25 and OX40 expression by mouse regulatory T cells.

CD40L and CD69 were then used in AIM assays to identify HYCAP-p15-specific  $T_{FH}$  cells and total BG505 Env-specific  $T_{FH}$  cells from BG505 Env trimer-immunized C57BL/6 mice (Fig. 2 C). We single-cell sorted HYCAP-p15-specific CD40L<sup>+</sup>CD69<sup>+</sup>CXCR5<sup>+</sup>PD-1<sup>+</sup>  $T_{FH}$  cells from three independent C57BL/6 mice, 8 d after immunizing with the BG505 Env trimer. The HYCAP-p15  $T_{FH}$  cells from two of the mice were subjected to single-cell RNA sequencing (scRNA-seq) to obtain paired TCR $\alpha/\beta$  sequences (Fig. S1 D). The TCR sequences were diverse, but the use of TRBV15 (International ImmunoGeneTics information system [IMGT] nomenclature) was highly elevated (~37%) relative to unimmunized C57BL/6 (~3%; Fig. 2, D and G; and Fig. S2). One TRBV15/TRAV12-3 TCR pair clonotype was observed multiple times in both mice (Fig. 2 E). We named this paired TCR sequence HYCAP1 (Fig. 2 F). A second TCR pair was selected according to the most frequently used TCR $\beta$  and TCR $\alpha$  V genes, TRBV15 and TRAV9-1. Among candidate sequences, although identical TCR $\beta$  CDR3 sequences were not found in the two independent mice, identical TCR $\alpha$  sequences could be found among TRBV15/TRAV9-1 paired TCRs in both mice. The recurring TCR $\alpha$  chain was paired with one of the naturally paired TRBV15 TCR $\beta$  sequences, distinct from the HYCAP1 TCR $\beta$ . We designated this sequence HYCAP3 (Fig. 2 F).

We generated two TCR Tg mouse lines, each expressing the HYCAP1 and HYCAP3 TCRs. Both mice were generated on a C57BL/6 background. In the founder mice, >80% of peripheral CD4 T cells expressed the Tg TCR $\beta$  gene, TRBV15 (Fig. 2 G), more commonly known as V $\beta$ 12 (and referred to as such from here on). Analysis of the spleen and thymus of the progeny mice showed a developmental pattern similar to that in other established CD4 Tg TCR mice, exhibiting increased CD4<sup>+</sup>CD8<sup>+</sup> thymocytes concomitantly observed with reduced CD8<sup>+</sup>CD4<sup>+</sup> and CD4<sup>+</sup>CD8<sup>+</sup> populations due to the Tg TCR enforced CD4 T cell

bias (Oxenius et al., 1998; Barnden et al., 1998), albeit with incomplete allelic exclusion (Fig. S2 A), resulting in ~75–90% of splenic CD4 T cells being V $\beta$ 12<sup>+</sup>V $\alpha$ 2<sup>+</sup> (Fig. S2 B). HYCAP3 TCR-expressing CD4 T cells had slightly reduced expression of total TCR $\beta$  compared with WT CD4 T cells, whereas TCR $\beta$  expression level on HYCAP1 CD4 T cells was slightly increased (Fig. S2 B). There was no abnormal development of HYCAP1 and HYCAP3 thymic CD25<sup>+</sup>Foxp3<sup>+</sup>  $T_{Reg}$  cells, confirming that these HYCAP TCRs were not self-reactive (Fig. S2 A).

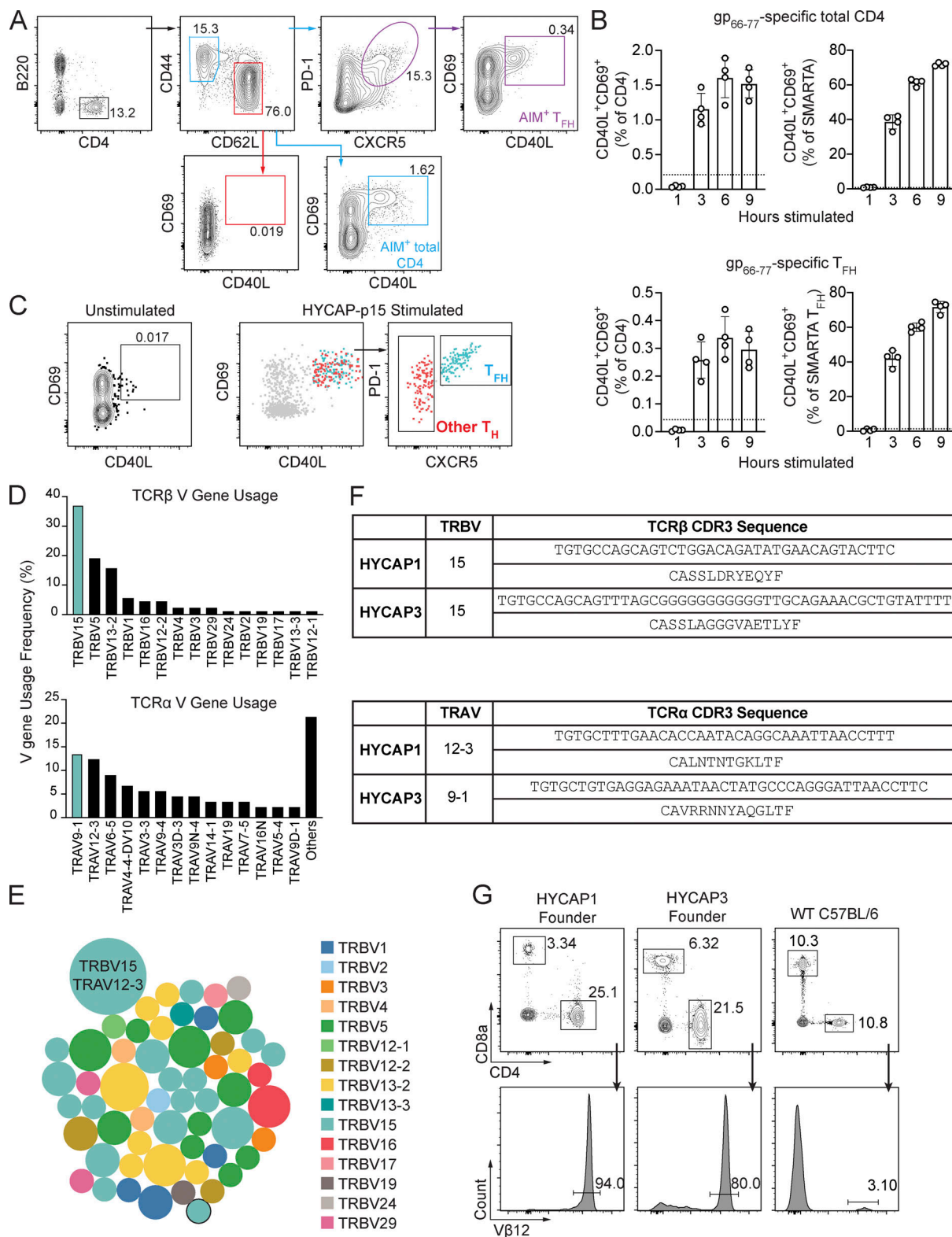
Affinity hierarchies of the HYCAP1 and HYCAP3 Tg TCRs compared with the polyclonal Env-specific response were measured by fluorescent tetramer titration (Keck et al., 2014). We generated an I-A<sup>b</sup> MHC class II tetramer presenting the 9-mer peptide SFEPIPIHY (HYCAP-p9:MHCII), which is what we predicted to be the HYCAP Tg core epitope (Fig. S3, A and B). This recombinant tetramer contains mutations in the I-A<sup>b</sup> molecule that enhance binding to CD4 (T. Dileepan and M.K. Jenkins, unpublished data). We tested the binding of HYCAP1 and HYCAP3 Tg CD4 T cells to different dilutions of HYCAP-p9:MHCII (Fig. S3, C and D) and calculated the concentration of tetramers at which 50% of the total HYCAP-p9:MHCII-specific T cells remained bound (half-maximal effective concentration [EC<sub>50</sub>]). The binding EC<sub>50</sub> was determined to be ~2.5 nM for HYCAP1 and 1.1 nM for HYCAP3 (Fig. S3 F). To perform the same assay against polyclonal CD4 T cells against the same epitope, we immunized C57BL/6 mice with the Env trimer to first expand the antigen-specific CD4 T cell response. 7 d after immunization, splenocytes were stained with different titrations of the same HYCAP-p9:MHCII (Fig. S3, E and G). The EC<sub>50</sub> of the polyclonal response was varied but was on average 3.1 nM to the HYCAP-p9:MHCII (Fig. S3 H). Thus, the relative affinities of HYCAP1 and HYCAP3 Tg TCR for HYCAP-p9:MHCII were similar to the polyclonal C57BL/6 CD4 T cell response.

### Increase in antigen-specific CD4 T cells enhances rare B cell responses

We sought to investigate the role of T cell help in a system where (a) the precursor frequency of target B cells is similar to bnAb precursor B cell frequencies in humans, and (b) the immunogen elicits an immunodominant response that the bnAb-class B cells must compete with. To do so, we designed a stabilized soluble BG505 SOSIP-trimer immunogen (Steichen et al., 2016) with germline targeting (GT) mutations (Briney et al., 2016) that confer high affinity to VRC01<sup>gHL</sup> (~89 nM monovalent dissociation constant [K<sub>D</sub>]). We call this immunogen MD39-GT3.1 (unpublished data). Previously, we established a rare bnAb B cell precursor frequency model by transferring a controlled number of congenically marked B cells expressing the inferred germline BCR of the bnAb VRC01 (VRC01<sup>gHL</sup>), which recognizes the CD4 binding site (CD4bs) of Env. Because WT mice are unable to generate VRC01-type responses (West et al., 2012; Jardine et al., 2013), in mice immunized with an immunogen with the CD4bs engineered to have high affinity to the VRC01<sup>gHL</sup> BCR, only the adoptively transferred VRC01<sup>gHL</sup> B cells can bind the CD4bs epitope in a bnAb-like manner (Abbott et al., 2018).

To determine if increasing the quantity of antigen-specific CD4 T cells can aid recruitment and proliferation of rare





**Figure 2. Identification and analysis of Env-specific CD4 T cell TCRs.** (A and B)  $5 \times 10^4$  SMARTA CD4 T cells ( $CD45.1^+$ ) were adoptively transferred into WT C57BL/6 mice, which were then immunized i.p. with KLH-gp<sub>61</sub>. Mice were sacrificed on day 8, and  $CD40L^+$  and  $CD69^+$  were tested as AIM markers on cells restimulated with 5  $\mu$ g/ml gp<sub>66-77</sub> peptide. One representative of several similar experiments is shown. (A) Representative flow cytometry plots showing gating strategy for identifying gp<sub>61</sub>-specific total CD4 T cells and gp<sub>61</sub>-specific  $T_{FH}$  cells. Figure shows staining 6 h after stimulation. Frequencies shown in AIM gates are percentages of AIM<sup>+</sup> CD4 T cells. (B) AIM<sup>+</sup> SMARTA CD4 T cells (blue gate in A) and  $T_{FH}$  cells (purple gate in A) can be detected ~6–9 h after restimulation. Mean and SD are shown. Dotted lines indicate average background signal from unstimulated cells after 9 h of culture. (C) Representative example flow plot of unstimulated  $CD40L^+CD69^+$   $T_{FH}$  cells from the spleen (gated on  $CD4^+/CD44^+CD62L^-/CXCR5^+PD-1^+$ ) and index sorted HYCAP-p15-specific AIM<sup>+</sup>  $T_{FH}$

(blue dots, CD4<sup>+</sup>/CD44<sup>+</sup>/CD40L<sup>+</sup>CD69<sup>+</sup>/CXCR5<sup>+</sup>PD-1<sup>+</sup>) and non-T<sub>FH</sub> CD4 helper cells (red dots, CD4<sup>+</sup>/CD44<sup>+</sup>/CD40L<sup>+</sup>CD69<sup>+</sup>/CXCR5<sup>-</sup>) that were restimulated for 5 h with HYCAP-p15, 8 d after immunization with the BG505 Env trimer. Gray dots are from total events collected before starting the index sort. The complete sort gating strategy showing parent gates can be found in Fig. S1 D. Frequency shown in the AIM<sup>+</sup> gate in the unstimulated condition is percentage of AIM<sup>+</sup> CD4 T cells. (D) Distribution of TCR $\beta$  and TCR $\alpha$  variable gene usage among HYCAP-p15-specific TCRs from sequenced T<sub>FH</sub> cells. The column "Others" in the TCR $\alpha$  distribution graph indicates unique TCR $\alpha$  V genes observed only once. Variable gene names follow the IMGT nomenclature.  $N = 1$ ,  $n = 89$ , where  $N$  corresponds to number of independent experiments and  $n$  represents the number of mice per group in a given experiment, pooled from two mice. (E) Bubble plot showing TCR $\beta$  VDJ-TCR $\alpha$  VJ paired clonotype distribution of TCRs shown in D. Bubbles are colored by TRBV gene. Relative size of the bubbles indicates the number of clonotypes, with the size of the outlined circle corresponding to one clonotype. (F) Nucleotide and amino acid sequences of HYCAP1 and HYCAP3 TCR $\alpha$  and TCR $\beta$  CDR3. (G) Flow cytometry of PBMCs of the Tg HYCAP1 and HYCAP3 founder mice, and a WT C57BL/6 mouse.

precursor B cells, we cotransferred  $5 \times 10^3$  to  $10^5$  HYCAP1 or HYCAP3 CD4 T cells along with a number of VRC01<sup>gHL</sup> B cells that results in establishment of a human-like precursor frequency (1 VRC01<sup>gHL</sup> B cell per  $10^6$  total splenic B cells; Abbott et al., 2018), followed by i.p. immunization with MD39-GT3.1 Env trimer (Fig. 3 A and Fig. S4). 10 d after immunization, the HYCAP CD4 T cells proliferated robustly in response to the immunization and were able to differentiate into Bcl6<sup>+</sup>CXCR5<sup>+</sup> GC-T<sub>FH</sub> cells (Fig. 3 B and Fig. S4 A). By AIM assay, an approximately two- to fourfold increase in the Env-specific CD4 T cell response was observed (Fig. 3, C–E; and Fig. S4 B), with approximately half or more of Env-specific cells being HYCAP1 or HYCAP3 CD4 T cells in the  $25 \times 10^3$  and  $10^5$  transfer groups (Fig. 3 E and Fig. S4 B). The HYCAP cells also constituted a substantial fraction of the Env-specific T<sub>FH</sub> cells, but an overall increase in Env-specific T<sub>FH</sub> was not observed (Fig. 3, F–H; and Fig. S4 C). Although the magnitude of the total GC response was essentially unchanged (Fig. 3, I and J), the change in total Env-specific CD4 T cells increased the abundance of the rare precursor VRC01<sup>gHL</sup> B cells in GCs. The number of VRC01<sup>gHL</sup> B<sub>GC</sub> cells in the GC increased ~33-fold after transfer of  $25 \times 10^3$  HYCAP1 CD4 T cells relative to the no-T-cell-transfer control (Fig. 3 K).  $5 \times 10^3$  and  $10^5$  HYCAP1 CD4 T cells also led to an increase in VRC01<sup>gHL</sup> B<sub>GC</sub> cells, although not as much as in the  $25 \times 10^3$  transfer condition (~6- and ~11-fold, respectively). Similar patterns were observed after transfer of HYCAP3 CD4 T cells (Fig. S4, D–F). Overall, we find that increasing the quantity of CD4 T cell help can create a GC response with greatly increased participation by rare precursor B cells.

#### CD4 T cells augment recruitment of rare B cells to the GC

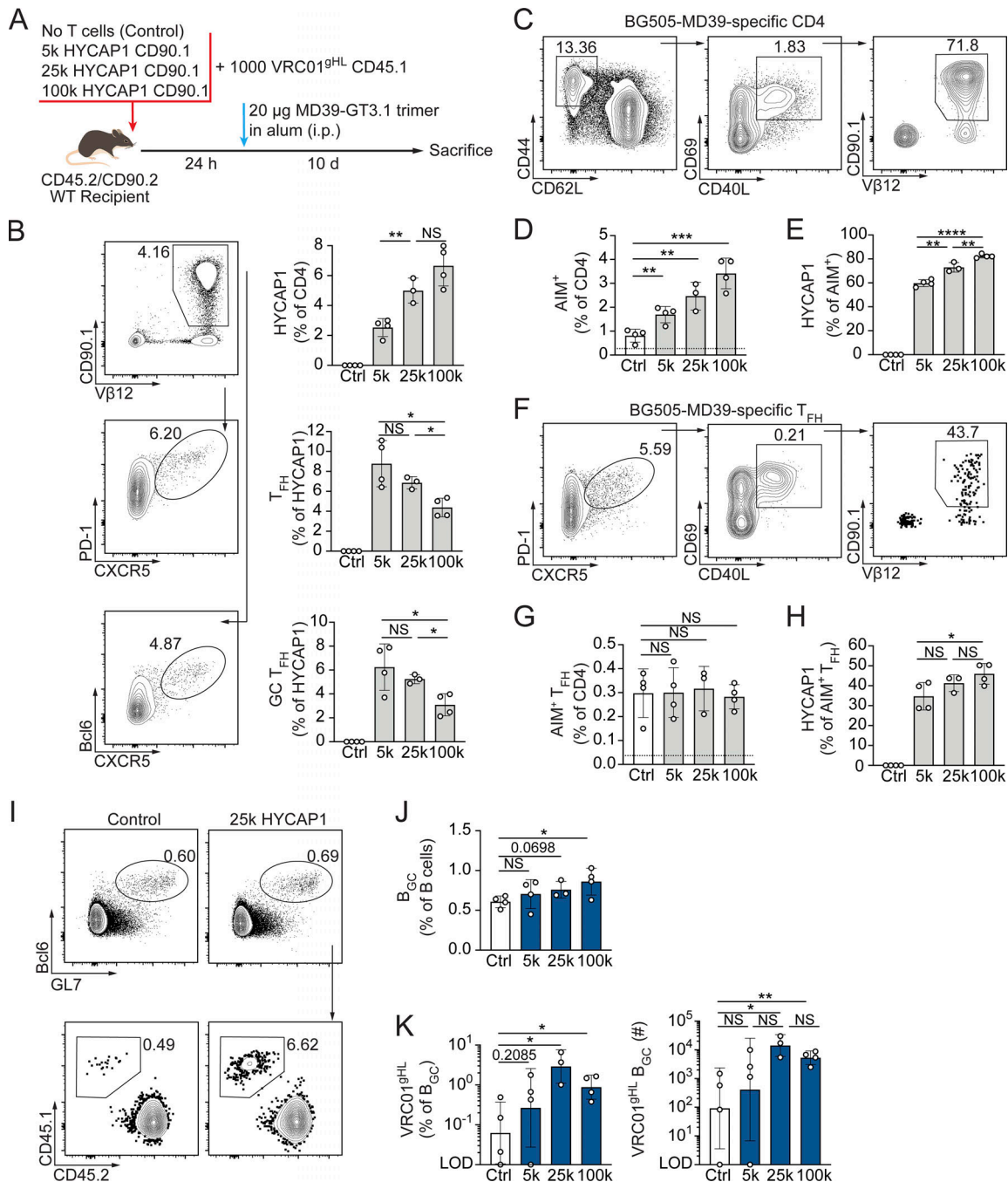
CD4 T cell responses generally peak earlier than B<sub>GC</sub> responses. Thus, the enhancement in VRC01<sup>gHL</sup> B<sub>GC</sub> frequencies may be a result of improved competitive fitness of rare cells once the GCs are fully established, or alternatively, T cell help may have enhanced the initial recruitment of those rare B cells to the GC. To test these possibilities, we examined T and B cell responses at an earlier time point after immunization. After transfer of  $10^3$  VRC01<sup>gHL</sup> B cells with or without  $25 \times 10^3$  HYCAP1 or HYCAP3 CD4 T cells, mice were immunized with the MD39-GT3.1 trimer. Splenocytes were analyzed 5 d after immunization to inspect recruitment of VRC01<sup>gHL</sup> to early GCs. Data points from the HYCAP1 and HYCAP3 groups were pooled to increase statistical power, as HYCAP1 and HYCAP3 mice behaved similarly. In the HYCAP recipient groups, GL7<sup>+</sup>Fas<sup>+</sup> early B<sub>GC</sub> frequencies were significantly increased (Fig. 4 A). VRC01<sup>gHL</sup> B<sub>GC</sub> frequencies were increased approximately fivefold, and the numbers of

VRC01<sup>gHL</sup> B<sub>GC</sub> were elevated approximately eightfold (Fig. 4 B). Notably, the rare early VRC01<sup>gHL</sup> B<sub>GC</sub> cells were detected much more consistently in the increased T help conditions compared with the normal C57BL/6 response. Total VRC01<sup>gHL</sup> B cell numbers also showed an approximately eightfold increase after HYCAP transfer (Fig. 4 C). HYCAP recipient mice generated an ~1.7-fold larger overall Env-specific CD4 T cell responses by day 5 (Fig. 4 D). The majority of Env-specific CD4 T cells and T<sub>FH</sub> cells were HYCAP cells (Fig. 4, D and E), confirming that the HYCAP cells dominated the CD4 T cell response early and were the main CD4 T cells recruiting VRC01<sup>gHL</sup> B cells to GCs.

#### Glycosylation affects accessibility to potential class II epitopes

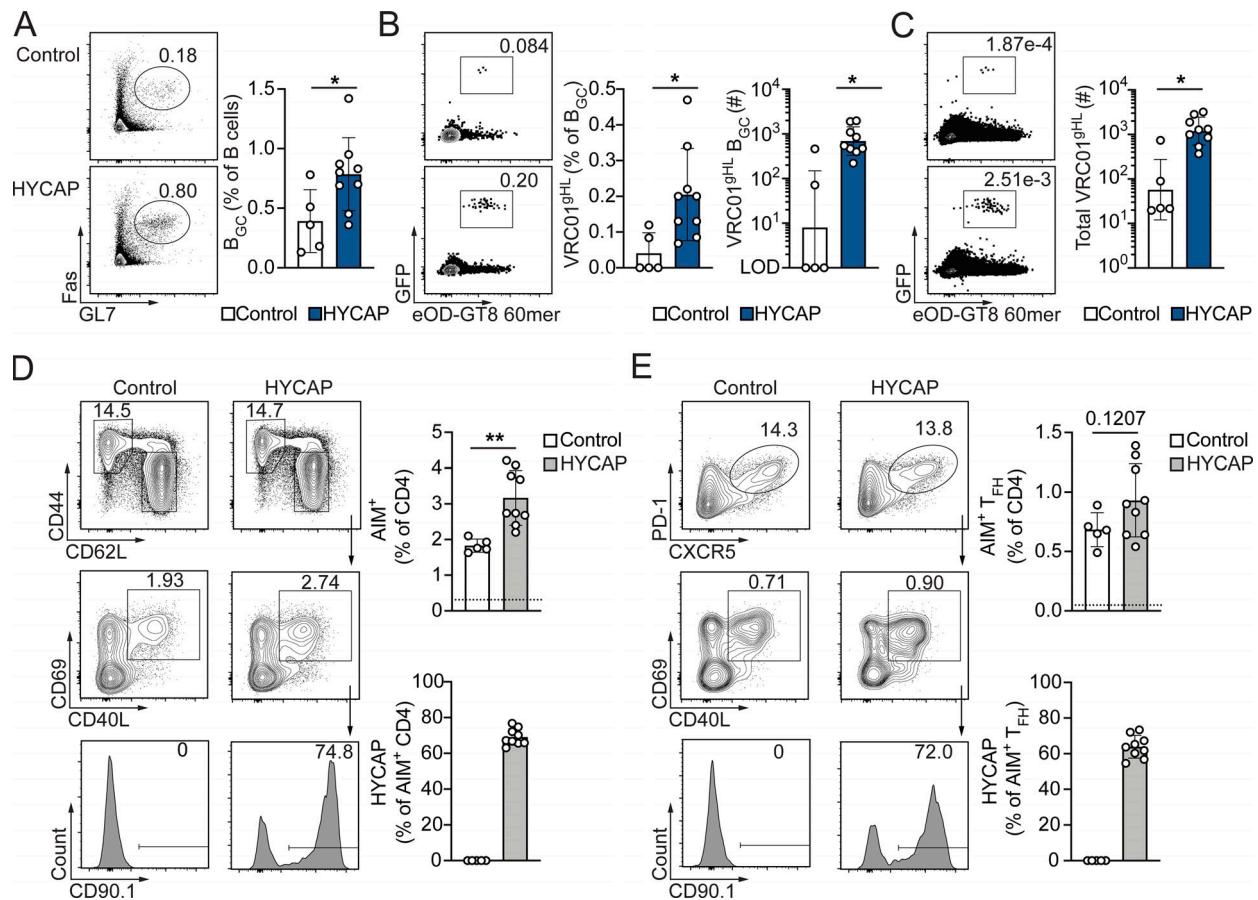
Unexpectedly, the frequency of Env-specific CD4 T cells in the C57BL/6 mice was found to already be close to 2% of total CD4 T cells on day 5 (Fig. 4 D), indicating that the magnitude of the early Env-specific CD4 T cell response in C57BL/6 mice was not as constrained as originally thought. To reassess immunodominant T helper epitopes within the BG505/MD39 Env sequence, we looked for potential I-A<sup>b</sup> restricted epitopes in the MD39 Env trimer sequence via the Immune Epitope Database (IEDB) MHC class II epitope prediction tool (Vita et al., 2019; Dhanda et al., 2019). 15-mer peptide fragments that were predicted to be the top-10th-percentile I-A<sup>b</sup> binders could be clustered into five main regions of Env (Fig. 5 A and Table S1). Regions 1–3 were in gp120, and regions 4 and 5 were in gp41. Two of the predicted hotspots contained conserved N-glycosylation sites: N243 in region 2 and N611 near the disulfide loop of Env in region 5, because the MHC class II peptide binding-prediction algorithm does not account for posttranslational modifications or TCR affinity, even though large glycans would be expected to prevent peptide recognition by CD4 T cells (Fig. 5 B).

We next assessed whether any of the five predicted epitope hotspots in Env were recognized in the context of a native-like Env trimer protein immunization. C57BL/6 mice were immunized with MD39-GT3.1 Env trimer. On day 10, the magnitude of the CD4 T cell response to each of the epitope-spanning 15-mer peptide pools (two to three peptides in each pool, none of which are glycosylated) was compared with the total Env-specific response by ICS (Fig. 5, C and D). Mice immunized with two different adjuvants (Alhydrogel alum and Sigma adjuvant) were analyzed. In both immunization conditions, only region 1, which included HYCAP-p15, and region 5 were consistently recognized (Fig. 5 D). Approximately 17–26% of the total Env-specific CD4 T cell response was directed toward region 1 (Fig. 5 D), consistent with our earlier observations (Fig. 1). Surprisingly, region 5 was clearly the immunodominant epitope, accounting for ~35–80%



**Figure 3. B/T cell cotransfer model of VRC01-class B cell responses. (A)** Experimental schematic.  $10^3$  VRC01<sup>gH</sup> B cells were cotransferred with the indicated varying numbers of HYCAP1 or HYCAP3 (Fig. S3) CD4 T cells into WT C57BL/6 recipients, then immunized i.p. with the MD39-GT3.1 trimer.  $N = 2$ ,  $n = 3-4$ , where  $N$  corresponds to number of independent experiments and  $n$  represents the number of mice per group in a given experiment. A representative experiment is shown. **(B)** Frequency of in vivo proliferated HYCAP1 CD4 T cells (CD90.1<sup>+</sup>Vβ12<sup>+</sup>) and the fraction of those HYCAP1 cells that are T<sub>FH</sub> (PD1<sup>+</sup>CXCR5<sup>+</sup>) or GC T<sub>FH</sub> (Bcl6<sup>+</sup>CXCR5<sup>+</sup>) cells. **(C–H)** Splenocytes were restimulated ex vivo for 5 h with BG505-MD39 MP. Frequencies shown in AIM gates are percent AIM<sup>+</sup> of CD4 T cells. **(C)** Gating strategy for AIM<sup>+</sup> CD4 T cells. **(D)** Total Env-specific CD4 T cells (gated as CD4<sup>+</sup>/CD44<sup>+</sup>CD62L<sup>+</sup>/CD40L<sup>+</sup>CD69<sup>+</sup>). **(E)** Proportion of AIM<sup>+</sup> CD4 T cells that are HYCAP1 CD4 T cells (CD90.1<sup>+</sup>Vβ12<sup>+</sup>). **(F)** Gating strategy for Env-specific T<sub>FH</sub> cells. **(G)** Total Env-specific T<sub>FH</sub> cells (gated as CD4<sup>+</sup>/CD44<sup>+</sup>CD62L<sup>+</sup>/CXCR5<sup>+</sup>PD1<sup>+</sup>/CD40L<sup>+</sup>CD69<sup>+</sup>). **(H)** Proportion of AIM<sup>+</sup> T<sub>FH</sub> cells that are HYCAP1 CD4 T cells (CD90.1<sup>+</sup>Vβ12<sup>+</sup>). **(I)** Flow cytometry of B<sub>GC</sub> cells (gated as B220<sup>+</sup>/Bcl6<sup>+</sup>GL7<sup>+</sup>) and VRC01<sup>gH</sup> B<sub>GC</sub> cells (gated as CD45.1<sup>+</sup>CD45.2<sup>+</sup> within B<sub>GC</sub>). **(J)** Frequency of total B<sub>GC</sub> cells (gated as B220<sup>+</sup>/Bcl6<sup>+</sup>GL7<sup>+</sup>). **(K)** Frequency and number of VRC01<sup>gH</sup> B<sub>GC</sub> cells. VRC01<sup>gH</sup> B<sub>GC</sub> cell number was back-calculated using the number of lymphocyte events collected and total number of lymphocytes enumerated from the spleen. Limit of detection (LOD) indicates that no VRC01<sup>gH</sup> cells were observed. Mean and SD are shown for data plotted on a linear axis. Geometric mean and geometric SD are shown for data plotted on a log axis. Representative flow plots are from the  $25 \times 10^3$  HYCAP1 transfer group unless indicated otherwise. NS,  $P > 0.05$ ; \*,  $P \leq 0.05$ ; \*\*,  $P \leq 0.01$ ; \*\*\*,  $P \leq 0.001$ ; \*\*\*\*,  $P \leq 0.0001$  (unpaired two-tailed Student's  $t$  test). Ctrl, control.





**Figure 4. T cell help enhances early GC formation and VRC01<sup>gH</sup> B cell proliferation.** (A–E)  $10^3$  GFP<sup>+</sup> VRC01<sup>gH</sup> cells were transferred alone or co-transferred with  $25 \times 10^3$  HYCAP1 or HYCAP3 cells into WT C57BL/6 recipients and immunized i.p. with 20  $\mu$ g MD39-GT3.1 trimer. HYCAP indicates data combined from HYCAP1 and HYCAP3 transferred mice.  $N = 2$ ,  $n = 4$ –5, where  $N$  corresponds to number of independent experiments and  $n$  represents the number of mice per group in a given experiment. A representative experiment is shown. (A and B) Early B<sub>GC</sub> (B220<sup>+</sup>/Fas<sup>+</sup>GL7<sup>+</sup>) cells (A) and VRC01<sup>gH</sup> B<sub>GC</sub> cells (GFP<sup>+</sup>eOD-GT8 60mer<sup>+</sup> gated on B<sub>GC</sub>; B). eOD-GT8 60mer is a VRC01-specific probe (Jardine et al., 2016), and is directly conjugated to Alexa Fluor 647 (Kato et al., 2020). The number of VRC01<sup>gH</sup> cells was back-calculated using the number of lymphocyte events collected and total number of lymphocytes counted from the spleen. (C) Total GFP<sup>+</sup>eOD-GT8 60mer<sup>+</sup> cells among B cells in the spleen on day 5. (D and E) Splenocytes were restimulated ex vivo for 5 h with BG505-MD39 MP. Frequencies shown in AIM gates are percent AIM<sup>+</sup> of CD4 T cells. AIM<sup>+</sup> cells were defined and gated as indicated in Fig. 3. (D) Frequency of MD39-specific CD4 T cells analyzed by AIM assay. (E) Frequency of MD39-specific T<sub>FH</sub> cells analyzed by AIM assay. Mean and SD are shown where data are plotted on a linear axis. Geometric mean and geometric SD are shown where data are plotted on a log axis. NS,  $p > 0.05$ ; \*,  $p \leq 0.05$ ; \*\*,  $p \leq 0.01$  (unpaired two-tailed Student's  $t$  test). Limit of detection (LOD) indicates that no VRC01<sup>gH</sup> cells were observed.

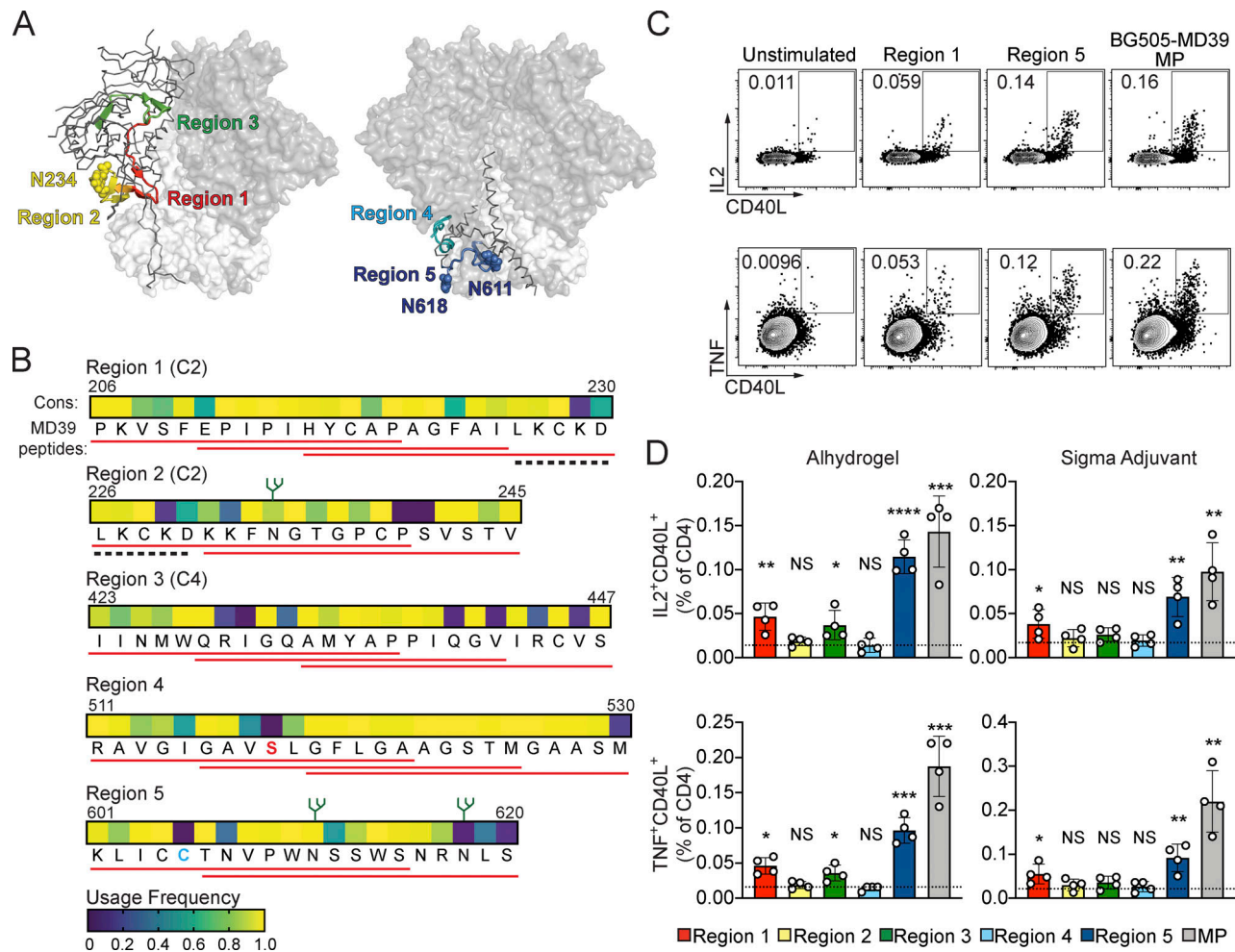
of the total Env-specific response, even though N611 is predicted to be N-glycosylated in trimeric Env proteins. In contrast, region 2 (overall ranked better than region 5 by the prediction algorithm) also contains an N-linked glycosylation site and failed to be recognized by CD4 T cells. It has been suggested that glycans on gp41 are underoccupied compared with glycans on gp120 when expressed as recombinant protein on both native-like SOSIP trimers (Guttmann et al., 2014; Depetris et al., 2012; Cao et al., 2018; Behrens et al., 2016) and uncleaved recombinant gp140 (Pabst et al., 2012; Go et al., 2011). The N611 glycosylation site, which falls within region 5, has been directly shown to be underglycosylated depending on the Env isolate (Cottrell et al., 2020; Cao et al., 2018).

#### Quantity of T cell help in T<sub>FH</sub>-deficient models is correlated with proliferation of rare B cells

There was a substantially large early endogenous CD4 T cell response against Env in C57BL/6 mice, with a region in gp41

constituting the immunodominant MHC class II response. As early CD4 T cell responses play a prominent role in the subsequent B<sub>GC</sub> response, we sought to investigate the impact of augmenting early CD4 T cell help in a model system in which the only source of antigen-specific CD4 T cells would be the Tg HYCAP CD4 T cells. Thus, we cotransferred varying numbers of congenically marked HYCAP1 CD4 T cells along with a physiological number of VRC01<sup>gH</sup> B cells into OTII Tg TCR recipient mice, which are unable to generate Env-specific CD4 T cell responses, followed by immunization with MD39-GT3.1 trimer (Fig. 6 A). HYCAP1 CD4 T cells proliferated in this model in response to the immunization (Fig. 6 B), and low HYCAP1 CD4 T cell transfer conditions ( $500$  and  $2 \times 10^3$ ) were sufficient to support a GC response in host animals. Transfers of more Env-specific T cells caused modest changes in the magnitude of the overall GC response (Fig. 6 C) but resulted in significant improvement in the recruitment of rare VRC01<sup>gH</sup> B cells to GCs compared with conditions with limited T cell help





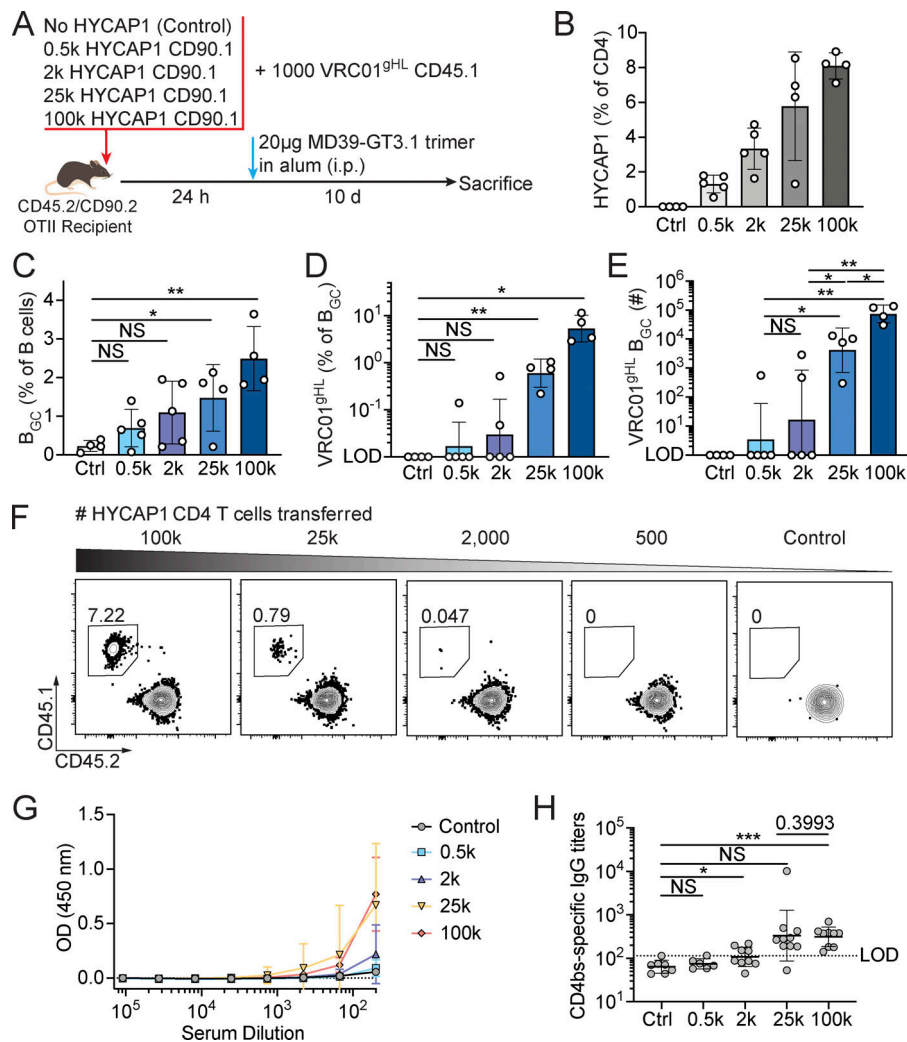
**Figure 5. Immunodominant CD4 T cell response may be driven by incomplete glycan occupancy.** (A) BG505-MD39 sequences covering regions with top 10th percentile binding to I-A<sup>b</sup> by IEDB prediction. Predicted gp120 (left) and gp41 (right) epitope hotspots are shown on the BG505 Env trimer structure (PDB: 4TVP). N-linked glycans within the epitopes are shown as spheres. (B) Sequence of regions indicated in A colored by residue usage frequency. Usage frequency indicates how conserved (Cons) is the exact amino acid residue in BG505-MD39, among known HIV group M Env sequences. Numbers above the sequences refer to amino acid residue position in HXB2 numbering. A 5-aa overlap between the C-terminus of region 1 and N-terminus of region 2 is indicated by dashed lines. N-linked glycosylation sites are indicated by cartoon branches. The red serine residue in region 4 is an MD39-specific stabilizing mutation, and the cysteine residue in blue is a SOSIP specific disulfide bond-forming mutation. (C and D) C57BL/6 mice immunized i.p. with MD39-GT3.1 trimer using the indicated adjuvant were sacrificed on day 10, and ICS was performed to identify I-A<sup>b</sup> MHC class II epitopes in BG505. Cells were restimulated for 5 h with the indicated peptide pool covering sequences shown in B.  $N = 2$ ,  $n = 4$ , where  $N$  corresponds to number of independent experiments and  $n$  represents the number of mice per group in a given experiment. (C) Flow cytometry plots of IL2<sup>+</sup>CD40L<sup>+</sup> and TNF<sup>+</sup>CD40L<sup>+</sup> CD4 T cells after 5-h peptide restimulation. Representative flow data shown is from alum adjuvanted mice restimulated with region 1 peptides, region 5 peptides, or BG505-MD39 MP. Frequencies shown for the cytokine gates are percent cytokine<sup>+</sup> of CD4 T cells. (D) Experiment in C quantified by indicated adjuvant used. Frequency of IL2<sup>+</sup>CD40L<sup>+</sup> CD4 T cells (top) and frequency of TNF<sup>+</sup>CD40L<sup>+</sup> CD4 T cells (bottom) after peptide stimulation. Mean and SD are shown. Statistics indicate pairwise comparison between the unstimulated condition and peptide pool tested. NS,  $> 0.05$ ; \*,  $P \leq 0.05$ ; \*\*,  $P \leq 0.01$ ; \*\*\*,  $P \leq 0.001$ ; \*\*\*\*,  $P \leq 0.0001$  (unpaired two-tailed Student's *t* test).

availability (Fig. 6, D-F). Although total B<sub>GC</sub> frequency was improved only ~2-fold by transferring  $25 \times 10^3$  instead of  $500 \text{ HY-CAPI CD4 T cells}$ , the number of VRC01<sup>gHL</sup> B<sub>GC</sub> was increased by ~1,000-fold (Fig. 6 E). Additionally, the  $10^5 \text{ HYCAPI CD4 T cell transfer group}$  outperformed the  $25 \times 10^3$  transfer condition, with an ~10-fold improvement in VRC01<sup>gHL</sup> B<sub>GC</sub> numbers (Fig. 6 E). Thus, the VRC01<sup>gHL</sup> B<sub>GC</sub> response was much more affected in limiting Env-specific CD4 T cell conditions than the total Env-specific B<sub>GC</sub> response. Importantly, increased T cell help in our model system did not result in a strong plasmablast differentiation bias by VRC01<sup>gHL</sup> cells, as indicated by minimal differences in the total serum response on day 10 (Fig. 6 F). These results were

encouraging, because serum antibodies are generally undesirable in response to a GT priming HIV immunogen (Finney and Kelsoe, 2020). Overall, these findings showed that increasing quantities of antigen-specific CD4 T cells directly correlated with the recruitment and retention of rare B cells into a GC response, without significantly skewing B cell differentiation into plasmablasts compared with B<sub>GC</sub> pathways.

## Discussion

The role of T cell help in B<sub>GC</sub> immunodominance hierarchies has been a knowledge gap for vaccine immunology. Here, we



**Figure 6. Frequency of VRC01<sup>gHL</sup> B<sub>GC</sub> cells directly correlate with T cell help in T help-deficient recipient.** (A) 10<sup>3</sup> VRC01<sup>gHL</sup> B cells (CD45.1<sup>+</sup>) along with varying numbers of HYCAP1 CD4 T cells (CD90.1<sup>+</sup>) were adoptively transferred into OTII Tg TCR recipient mice (CD45.2<sup>+</sup>CD90.2<sup>+</sup>). Mice were immunized with 20 μg MD39-GT3.1 trimer adjuvanted with alum and sacrificed 10 d after immunization. *n* = 3, *n* = 3–5. A representative experiment is shown. (B) Frequency of total HYCAP1 CD4 T cells (CD90.1<sup>+</sup>Vβ12<sup>+</sup>) 10 d after immunization. (C) Frequency of B<sub>GC</sub> cells (gated as B220<sup>+</sup>/Bcl6<sup>+</sup>GL7<sup>+</sup>). (D) Frequency of VRC01<sup>gHL</sup> B<sub>GC</sub> cells (gated as CD45.1<sup>+</sup>CD45.2<sup>+</sup> within the B<sub>GC</sub> gate). (E) Number of VRC01<sup>gHL</sup> B<sub>GC</sub> cells. (F) Flow cytometry of VRC01<sup>gHL</sup> B<sub>GC</sub> cells 10 d after immunization (gated on B220<sup>+</sup>/Bcl6<sup>+</sup>GL7<sup>+</sup>). (G) CD4bs-specific serum IgG ELISA 10 d after immunization detected by using the eOD-GT8 RSF probe (Kato et al., 2020). *N* = 2, *n* = 3–5, where *N* corresponds to number of independent experiments and *n* represents the number of mice per group in a given experiment. (H) Endpoint titers calculated from the ELISAs performed in G. The LOD corresponds to the largest endpoint titer in the control condition. Mean and SD are shown where data are plotted on a linear axis. Geometric mean and geometric SD are shown where data are plotted on a log axis. NS, > 0.05; \*, *P* ≤ 0.05; \*\*, *P* ≤ 0.01; \*\*\*, *P* ≤ 0.001 (unpaired two-tailed Student's *t* test). Ctrl, control.

studied the role of CD4 T cell help in the competition between immunodominant versus rare physiological precursor frequency B cells in response to the HIV Env trimer, by controlling the precursor frequencies of both rare precursor B cells and Env-specific CD4 T cells. In developing our model system, we attempted to mimic a more physiological CD4 T cell response to Env by using newly generated CD4 Tg TCR mice that express TCRs naturally occurring among T<sub>FH</sub> cells in C57BL/6 mice after Env immunization. We found that by increasing the quantity of Env-specific CD4 T cells by adoptive transfer of Env-specific CD4 T cells, GC occupancy by rare precursor VRC01<sup>gHL</sup> B cells was improved. We observed that this occurred because the more numerous antigen-specific CD4 T cells were able to provide help early, likely during the recruitment of VRC01<sup>gHL</sup> B cells to the GC. Reports have previously demonstrated that pre-B<sub>GC</sub> cells with high surface peptide:MHC complex density are preferentially recruited into the GC owing to preferential T cell help, using haptenated antigens and abundant antigen-specific B and T cells (Schwickert et al., 2011; Yeh et al., 2018). These mechanisms are consistent with our observations in this model using rare B cells and a difficult protein antigen.

An encouraging outcome of our experiments was that the increase in T cell help did not preferentially aid the endogenous,

non-VRC01<sup>gHL</sup> B<sub>GC</sub> cells that are immunodominant. Of note, in our model system, the VRC01<sup>gHL</sup> precursor B cells have a relatively high affinity (*K<sub>D</sub>*: ~89 nM) to the MD39-GT3.1 trimer immunogen. This affinity is likely substantially better than that of the immunodominant B cells (Abbott and Crotty, 2020). Endogenous B cell responses to Env, including base-directed serum responses, are not readily detectable by flow cytometry using fluorescent Env probe staining at day 10, suggesting that the endogenous B<sub>GC</sub> responses typically comprise low-affinity B cells (unpublished data). On the other hand, authentic human bnAb precursor B cells to the GT immunogen eOD-GT8 (currently in phase I clinical trial: NCT03547245) generally possesses *K<sub>D</sub>* values of 0.1–100 μM (Havenar-Daughton et al., 2018; Jardine et al., 2016). Because affinity is a seminal factor in competing for T cell help (Schwickert et al., 2011) and in whether rare precursor B cells can be recruited to the GC (Abbott et al., 2018), it remains to be addressed what impact increasing CD4 T cell help would have in conditions of weaker GT affinities.

Env immunogens are notorious for not being particularly immunogenic (Klasse et al., 2020), and prolonged antigen delivery strategies have shown to enhance gp120- or Env trimer-specific responses (Tam et al., 2016; Cirelli et al., 2019). Maximum total B<sub>GC</sub> and T<sub>FH</sub> responses, especially at typical

peak GC (around day 10 in mice) and later time points, are likely limited by antigen availability (Deenick et al., 2010; Baumjohann et al., 2013) because of rapid dispersion of Env after immunization (Tokatlian et al., 2019; Cirelli et al., 2019).  $10^5$  HYCAP CD4 T cell transfers in C57BL/6 mice, in combination with the endogenous polyclonal Env-specific CD4 T cells, likely resulted in a much earlier and larger peak of the total CD4 T cell response. Such a large prevalence of Env-specific CD4 T cells may have improved activation of rare VRC01<sup>gHL</sup> B cells during the pre-GC stages. In our OTII recipient system, in which the transferred HYCAP1 CD4 T cells were the only source of antigen-specific CD4 T cells,  $10^5$  HYCAP1 CD4 T cell transfer resulted in the highest day-10 VRC01<sup>gHL</sup> B<sub>GC</sub> response, indicating that an increase in T cell help preferentially augments rare B cell recruitment to the GC.

Finally, we found that the immunodominant MHC class II Env epitope in C57BL/6 mice was in gp41 encompassing residues 601–620, a region that contains two N-linked glycosylation sites, N611 and N618. Glycosylated peptides can be recognized by both CD4 and CD8 T cells, but known responses to glycosylated peptides are rare, and demonstration of this has been largely limited to peptides carrying small glycans with only one to three saccharide subunits (Sun et al., 2016). It is relatively less known what role large N-linked glycans such as those on Env have on MHC peptide processing, presentation, and recognition by TCR. One recent study showed direct evidence that a CD4 T cell epitope containing a paucimannose glycan at N187 is presented and recognized to facilitate T cell help to B cells (Sun et al., 2020). Likewise, a second recent study that directly identified CD4 T cell epitopes from severe acute respiratory syndrome coronavirus 2 (SARS-CoV-2) Spike glycoprotein presented on HLA-DR demonstrated that several presented epitope sequences contained paucimannose glycans that were smaller than the native glycoforms presented on the intact antigen, although the study did not confirm that CD4 T cells were indeed able to recognize those glycopeptide-loaded MHC class II molecules (Parker et al., 2020 Preprint). Neither study identified MHC class II presentation of highly branched complex glycans, suggesting that if glycopeptides are presented, they are trimmed down to their paucimannose core. In our experiments, the large ex vivo restimulation response from C57BL/6 mice to the nonglycosylated linear peptides in the gp41 601–620 region indicates that the in vivo presented and recognized epitope is not glycosylated. Similarly, in Balb/c mice, the P4-2 epitope contained the N197 N-linked glycosylation site, but CD4 T cells in that experiment produced cytokines in response to glycan-free peptides (Fig. 1, B and C). In C57BL/6 mice, CD4 T cells did not respond to an epitope in gp120 C2 with a conserved N-linked glycan, which, based on the peptide sequence, was predicted to be a well-presented MHC class II epitope. Hence, at least some of the Env-specific CD4 T cell responses are likely a result of suboptimal glycosylation on specific N-linked glycosylation sites. For example, N611 is thought to be underglycosylated in BG505 SOSIP Env trimers (Cottrell et al., 2020), and N197 was directly shown to be underglycosylated in BG505 SOSIP (Cao et al., 2018), although these results have yet to been shown in BG505 SOSIP trimer containing the MD39 trimer

stabilizing mutations. The large CD4 T cell response to the underglycosylated gp41 region 5 trimer variants might not be recapitulated when immunizing with other Env constructs that have a much higher glycan occupancy at N611. Region 5 was not an immunodominant epitope among HIV-infected patients, unlike HYCAP-p15 (Ranasinghe et al., 2012). Therefore, underglycosylation or glycan holes on Env trimer vaccine candidates may influence not only B cell, but also MHC class II, responses. As others have noted, these observations also highlight the importance of identifying the proper glycosylation states presented on immunogens currently being developed as HIV vaccine candidates (Seabright et al., 2019). These glycan hole-influenced immunodominant MHC class II responses should be taken into consideration when compiling a vaccination schedule using multiple sequential boosts with different antigens, if attempting to recall memory CD4 T cell responses.

Overall, we demonstrate that one possible strategy to overcoming immunodominance is by immunization approaches that can increase early T cell help availability to B cells, especially when combined with immunogens that are designed to have high affinity for rare B cells. As such, to elicit rare B cell responses, vaccination strategies that can efficiently prime antigen-specific CD4 T cell responses without activating immunodominant B cells are worthy of exploration.

## Materials and methods

### Immunogen expression and purification

Env trimers were produced as previously described (Steichen et al., 2016). Briefly, the trimers were expressed in HEK293F cells by transient transfection. 5–7 d after transfection, protein was purified from the supernatant using a HiTrap NHS-Activated HP affinity column (GE Healthcare) conjugated to bnAb, 2G12, or PGDM1400. The eluent from antibody affinity chromatography was size-exclusion purified using a S200 Increase 10–300 column (GE Healthcare) in Tris-buffered saline (50 mM Tris, pH 7.4, and 150 mM NaCl) and concentrated to 1 mg/ml. The purified protein was aliquoted and frozen at  $-80^{\circ}\text{C}$  until use.

### Mice and immunizations

Depending on the experiment, B cells from congenically marked VRC01<sup>gHL</sup> mice (GFP<sup>+</sup>, CD45.1/CD45.2, or CD45.1/CD45.1) were purified using the Stemcell EasySep Mouse B Cell Isolation Kit (Stemcell) according to the manufacturer's instructions. Three times the number of target VRC01<sup>gHL</sup> B cells to be transferred (correcting for one third of the total B cells in VRC01<sup>gHL</sup> Tg mice being CD4bs specific; Abbott et al., 2018) were retro-orbitally transferred into the recipient mice. In this study, to obtain a precursor frequency of 1 VRC01<sup>gHL</sup> in  $10^6$  B cells in the spleen,  $3 \times 10^3$  total B cells (equivalent to  $10^3$  VRC01<sup>gHL</sup> B cells) isolated from VRC01<sup>gHL</sup> mice were adoptively transferred. For B and T cell cotransfers, CD4 T cells from CD90.1<sup>+</sup> (either CD90.1/90.1 or CD90.1/90.2) HYCAP1 or HYCAP3 mice were purified using the Stemcell EasySep Mouse CD4<sup>+</sup> T Cell Isolation Kit (Stemcell). Recipient C57BL/6 and B6.Cg-Tg(Tcr $\alpha$ Tcr $\beta$ )425Cbn/J (OTII) mice were purchased from The Jackson Laboratory. The purified



HYCAP CD4 T cells checked by flow cytometry were typically ~80–90% V $\beta$ 12<sup>+</sup>, although the number of CD4 T cells transferred was not corrected for percentage V $\beta$ 12<sup>+</sup>. Different numbers of purified HYCAP CD4 T cells were cotransferred along with purified VRC01<sup>gHL</sup> cells, as indicated for each experiment. In initial AIM assay experiments,  $5 \times 10^4$  purified CD4 T cells from SMARTA CD45.1 mice from our in-house colony were retro-orbitally transferred. In all experiments, RPMI medium (Corning) containing 10% FBS was used as the transfer buffer. Transferred cells were sex matched with the recipient mice. Both male and female mice were used for experiments. Transferred cells were from mice that were 7–11 wk old. All recipient mice used were 7–9 wk old at the time of immunization.

All immunizations were performed by mixing 20  $\mu$ g of the specified immunogen diluted in PBS with 1 mg of Alhydrogel alum (InvivoGen) in a 200- $\mu$ l total volume, unless indicated otherwise. For experiments in which Sigma adjuvant (Sigma-Aldrich) was used, 20  $\mu$ g of immunogen was diluted in PBS up to 100  $\mu$ l and mixed with 100  $\mu$ l Sigma adjuvant for a single 200- $\mu$ l-volume injection. In cell transfer conditions, mice were immunized ~24 h after transfer. All mice were immunized i.p. unless indicated otherwise. All mice used in the study are on a C57BL/6 background, except for the Balb/c mice used in the ELISPOT assays. All mouse experiments were done with approval of the La Jolla Institute for Immunology (LJI) institutional animal care and use committee.

### Flow cytometry

Mice were sacrificed, and spleens were harvested at the indicated time points after immunization. Splenocytes were isolated from red blood cells by ammonium-chloride-potassium (ACK) lysis buffer (Gibco) and resuspended in FACS buffer (5% FBS in 1 $\times$  PBS). Cells were Fc blocked (clone 2.4G2; BD Biosciences) and stained with antibody master mix in FACS buffer for 30 min in the dark at 4°C. Secondary stains, where applicable, were also performed for 30 min in the dark at 4°C. After surface staining, cells were washed and fixed in Foxp3 fixation kit (eBioscience) for intranuclear staining or BD cytofix/cytoperm (BD Biosciences) for ICS or surface staining. Where applicable, intracellular markers were stained for 45 min to 1 h at 4°C. Samples were acquired on a BD LSRFortessa or BD FACSCelesta. All flow cytometry data were analyzed in FlowJo v10.

### Peptide pools and T cell restimulation assays

Env trimer peptide pools were generated as 15-mers spanning the entire construct sequence, overlapping by 10 residues. Individual peptides were resuspended in DMSO and stored at –30°C until use. To generate the BG505 or MD39 MP, equal amounts of each peptide were combined, lyophilized, and resuspended in DMSO at a concentration of 2 mg/ml of each peptide.

Spleens harvested from immunized mice were seeded at 1 million cells per well in flat-bottom 96-well plates and restimulated with 5  $\mu$ g/ml of single peptides or 2  $\mu$ g/ml BG505 or MD39 MP, along with an unstimulated control in D10 (DMEM, 10% FBS, 1 $\times$  penicillin/streptomycin, 1 $\times$  Glutamax, and 50  $\mu$ M 2-mercaptoethanol) for 5–9 h at 37°C in a humidity-controlled

CO<sub>2</sub> incubator. For ICS assays, 5  $\mu$ g/ml final concentration of brefeldin A (Sigma-Aldrich) was added into the stimulation medium. For AIM assays, anti-CD40L mAb (clone MRI) was labeled with Alexa Fluor 647 in-house using an Alexa Fluor 647 antibody labeling kit (Life Technologies) according to the manufacturer's instructions, and 0.5  $\mu$ g/ml final concentration of anti-CD40L-AlexaFluor647 was added to the stimulation medium.

### Tetramer generation and staining

Splenocytes from C57BL/6 mice receiving  $25 \times 10^3$  HYCAP1 or HYCAP3 CD4 T cells along with  $10^3$  VRC01<sup>gHL</sup> B cells 10 d after immunization with MD39-GT3.1 trimer were ex vivo restimulated for 5 h with HYCAP-p15 peptide or individual overlapping 11-mers partially comprising the HYCAP-p15 peptide sequence. All peptides were used at a final concentration of 5  $\mu$ g/ml. The core 9-mer epitope was deduced to be SFEPIPIHY based on the overlapping region identified in the 11-mers that were capable of restimulating the HYCAP1 and HYCAP3 CD4 T cells.

Recombinant high-affinity I-A<sup>b</sup> MHC class II tetramers (T. Dileepan and M.K. Jenkins, unpublished data) were generated with SFEPIPIHY as the loaded peptide sequence. The core 9-mer epitope was used instead of the full 15-mer to control for peptide loading variability among the independent MHC class II molecules used to form the tetrameric streptavidin complex. The HYCAP-p9:MHCII molecules were biotinylated and complexed with APC-SA to generate fluorescent tetramers. DIYKG-VYQFKSV:MHC class II I-A<sup>b</sup> (LCMV gp<sub>66</sub>:MHCII) complexed with BV421-SA were obtained from the Emory Tetramer Core. Splenocytes from naive HYCAP1 and HYCAP3 mice were stained with varying dilutions of the HYCAP-p9:MHCII tetramer along with a fixed dilution of an irrelevant gp<sub>66</sub>:MHCII tetramer (1:200 of a 1.3-mg/ml stock) in D10 for 1 h in a 37°C incubator. Cells were washed twice with FACS buffer and stained with additional antibodies for 30 min at 4°C. After staining with antibodies, cells were washed twice and fixed in BD Cytofix (BD Biosciences).

To quantify the binding of SFEPIPIHY-specific polyclonal CD4 T cells, C57BL/6 mice were immunized i.p. with 20  $\mu$ g MD39-GT3.1 trimer adjuvanted with alum, to first expand the number of antigen-specific CD4 T cells. 7 d after immunization, splenocytes were harvested and stained as described above.

### ELISPOTs

Balb/c mice were immunized s.c. in each footpad with 1  $\mu$ g BG505 SOSIP trimer in 0.1  $\mu$ g Abisco-100 (Novavax; Sun et al., 2009) and 3 wk later immunized with 1  $\mu$ g BG505 SOSIP trimer in 0.1  $\mu$ g Abisco-100 in each footpad, both sides of the base of the tail, and both sides of the interscapular region. Splenocytes of nonimmunized Balb/c mice were stimulated with LPS (6.25  $\mu$ g/ml final concentration) and dextran sulfate (7  $\mu$ g/ml final concentration) in R10 medium (RPMI, 10% FBS, 1 $\times$  penicillin/streptomycin, 1 $\times$  Glutamax, and 50  $\mu$ M 2-mercaptoethanol) and cultured at 37°C for 3 d. The APCs from the spleens were harvested, frozen, and stored in liquid nitrogen until further use.

Peptides were prepared as above and grouped into 8 pools of equal amounts of 10 consecutive peptides and 4 pools of equal amounts of 11 consecutive peptides. ELISPOT plates were

prepared as described previously (Oseroff et al., 2012). Briefly, ELISPOT plates were prepared the day before the assay, by plating 10  $\mu\text{g}/\text{ml}$  of anti-IFN $\gamma$  or anti-IL5 per well into flat-bottom 96-well nitrocellulose plates (Millipore). On the day of the assay, CD4 T cells were isolated from spleens and popliteal and inguinal LNs of the immunized mice using a MACS CD4 T cell isolation kit (Miltenyi Biotec) and resuspended in R10. Peptide pools were plated in wells at a final concentration of 10  $\mu\text{g}/\text{ml}$  ( $\sim 1 \mu\text{g}/\text{ml}$  per peptide) in 25  $\mu\text{l}$ . APCs were plated at  $10^5$  cells/well in 25  $\mu\text{l}$ , and the isolated CD4 T cells were added at  $4 \times 10^5$  cells/well in 100  $\mu\text{l}$ . After incubating overnight for 20 h, plates were washed, and spots were counted by computer-assisted image analysis (KS-ELISPOT reader; Zeiss).

### ELISAs

96-well half-area ELISA plates (Corning) were directly coated overnight at 4°C with 2  $\mu\text{g}/\text{ml}$  resurfaced eOD-GT8 immunogen (eOD-GT8-RSF) diluted in 1 $\times$  PBS. This immunogen displays the CD4bs and is designed to bind VRC01<sup>gHL</sup> Ig with high affinity, but otherwise does not share epitopes with the MD39-GT3.1 trimer immunogen (Jardine et al., 2016; Kato et al., 2020). The coated plates were washed five times with wash buffer (0.05% Tween-20 in 1 $\times$  PBS) and blocked for 1 h with 3% BSA in 1 $\times$  PBS at room temperature. Mouse serum serial titrations made in dilution buffer (1% BSA in 1 $\times$  PBS) were added to the ELISA plates for 1 h at room temperature. Recombinant VRC01<sup>gHL</sup> IgG was used to generate binding curves for normalization between plates. After primary antibody binding, plates were washed five times with wash buffer. Anti-mouse IgG-HRP secondary antibody (The Jackson Laboratory) for the mouse serum wells or anti-human IgG-HRP secondary antibody (The Jackson Laboratory) for the recombinant VRC01<sup>gHL</sup> IgG control wells was diluted in dilution buffer and added to the washed ELISA plates for 1 h at room temperature. After a final 5 $\times$  wash with the wash buffer, 1-Step Ultra TMB-ELISA solution (Thermo Fisher Scientific) was added for 5 min to detect binding. The reaction was then stopped with 1N H<sub>2</sub>SO<sub>4</sub>, and absorbance at OD 450 nm was measured on an EnVision ELISA plate reader (PerkinElmer).

### Cell sorting and TCR sequencing

Splenocytes harvested from three mice that were immunized with 20  $\mu\text{g}$  BG505 trimer adjuvanted with alum were restimulated for 5 h with 5  $\mu\text{g}/\text{ml}$  HYCAP-p15 peptide. Activated (CD44<sup>+</sup>CD62L<sup>-</sup>) HYCAP-p15-specific CD40L<sup>+</sup>CD69<sup>+</sup> T<sub>FH</sub> (CXCR5<sup>+</sup>PD1<sup>+</sup>) cells were index sorted on a FACSARIA II Cell Sorter using a 85- $\mu\text{m}$  nozzle on single-cell purity setting into the inner 60 wells of a 96-well half-skirted PCR plate (Bio-Rad) containing 4  $\mu\text{l}$  of lysis buffer (0.1% vol/vol Triton X-100, 4 U RNase inhibitor [New England Biolabs], and 2.5 mM dNTPs). HYCAP-p15-specific CD40L<sup>+</sup>CD69<sup>+</sup> non-T<sub>FH</sub> (CXCR5<sup>-</sup>) cells were sorted in a similar manner, as a backup population. Per mouse, two plates each were sorted for the two AIM<sup>+</sup> CD4 T cell subsets. Plates were immediately frozen on dry ice and stored at  $-80^\circ\text{C}$ .

To obtain TCR sequences from the sorted cells, we performed scRNA-seq on CD40L<sup>+</sup>CD69<sup>+</sup> T<sub>FH</sub> cell plates from two of the three mice (one T<sub>FH</sub> plate each from two mice), using a modified Smart-seq2 protocol described previously (Patil et al., 2018).

Briefly, reverse transcription products were preamplified for 23–24 PCR cycles and purified using 0.8 $\times$  Ampure XP beads (Beckman). Barcoded Illumina sequencing libraries (Nextera XT library preparation kit; Illumina) were generated from the preamplified cDNA. Libraries were sequenced on the HiSeq2500 Illumina platform to obtain 50-bp single-end reads (TruSeq Rapid Kit; Illumina). TCR genes were assembled and annotated using MiXCR (Bolotin et al., 2015). Cells without paired TCRs or with low read counts were filtered out.

To help identify second- and third-candidate sequences, some of the remaining frozen single-cell plates from both T<sub>FH</sub> and non-T<sub>FH</sub> plates were single-cell Sanger sequenced after targeted amplification of TCR $\alpha$  and  $\beta$  genes, using primers corresponding to the TRAV and TRBV genes most frequently observed in the RNA-seq data. Reverse transcription was performed directly on the single cell-sorted plates using SuperScript II (Life Technologies) according to the manufacturer's protocols. cDNA was amplified using cycling conditions and TCR-specific primers listed in Stubbington et al. (2016), with the barcoding and adaptor portions of the primers removed. The TCR $\beta$  gene was amplified using a pool of TCR $\beta$  primers including forward primers TRBV5, TRBV13, and TRBV15. The TCR $\alpha$  gene was amplified using a pool of TCR $\alpha$  primers, TRAV9\_1, TRAV4\_C, TRAV3, TRAV6\_4, and TRAV12\_1. The primer names listed here match the names reported in Stubbington et al. (2016). CDR3 sequences were analyzed to determine if the Sanger-sequenced cells matched clonotypes observed from scRNA-seq.

### Tg TCR mouse generation

Two paired TCR sequences were selected for injection into mice. The full TCR sequence including a Kozak sequence and native signal peptide was ligated into vectors containing a phCD2 promoter cassette with either a TCR $\alpha$  or TCR $\beta$  constant region (Zhumabekov et al., 1995). After the construct plasmids were confirmed by sequencing, the DNA was linearized and gel purified to remove the Bluescript SK(–) segment by digesting the plasmid with KpnI and NotI restriction sites. TCR gene DNA bands were isolated by QIAquick Gel Extraction Kit (Qiagen). The bands corresponding to the expression cassette containing TCR genes were provided to the University of California, San Diego Transgenic Mouse Core at 20 ng/ $\mu\text{l}$  in microinjection buffer (7.5 mM Tris-HCl, pH 7.4, and 0.15 mM EDTA), where the TCR $\alpha$ / $\beta$  pair DNA coinjection into blastocysts was performed. Potential Tg pups were transferred to the LJI vivarium. Mice were genotyped for the appropriate Tg TRAV and TRBV genes and phenotyped by checking for reduction in circulating CD8 T cells and dominant expression of V $\beta$ 12, which corresponds to TRBV15 in IMGT nomenclature. Anti-TCR $\alpha$  TRAV12-3 and TRAV9-1 antibodies were unavailable. Therefore, during phenotyping, reduction in the frequency of Va2-expressing CD4 T cells was used as an indirect indication of Tg TCR $\alpha$  expression, as Va2 is a highly used TCR $\alpha$  V gene in C57BL/6 mice. HYCAP3 and HYCAP1 Tg expressing founder mice originally on C57BL/6 background were crossed with CD90.1-expressing 6.PL-Thy1a/CyJ mice from The Jackson Laboratory. Thymocytes were analyzed from Tg<sup>+</sup> progeny mice and their Tg<sup>-</sup> littermate controls (defined by genotyping and phenotyping). Primers used for

genotyping are as follows: TRAV12-3 forward primer, 5'-CAG ACAACAAGAGGACCGAG-3'; TRAV9-1 forward primer, 5'-TAT GGTGGATCCATTACCTCTCC-3'; TRBV15 forward primer, 5'-GAAGTGTGAGCCAGTTTCAGG-3'; TCR $\alpha$  reverse primer, 5'-CAC AGCAGGTTCCGGATTC-3'; and TCR $\beta$  reverse primer, 5'-CTT GGGTGGAGTCACATTTCTC-3'.

### Statistical analysis

All data were plotted and analyzed in Prism 8 (GraphPad). Statistical significance between appropriate groups was tested by an unpaired, two-tailed Student's *t* test at a confidence level of 95%. P values are indicated as follows: NS,  $> 0.05$ ; \*,  $P \leq 0.05$ ; \*\*,  $P \leq 0.01$ ; \*\*\*,  $P \leq 0.001$ ; and \*\*\*\*,  $P \leq 0.0001$ .

### Online supplemental material

**Fig. S1** shows exploration of additional AIM markers and the complete gating strategy applied in single-cell sorting. **Fig. S2** shows T cell development and phenotyping of CD4 T cells in the Tg TCR HYCAP1 and HYCAP3 mouse lines generated in this study. **Fig. S3** presents core epitope mapping for HYCAP TCRs and relative affinity determination of the TCRs. **Fig. S4** is a replicate of the experiment performed in **Fig. 3** but using HYCAP3 CD4 T cells instead. Table S1 lists the top I-A<sup>b</sup> restricted MHC class II epitopes in BG505 Env, predicted by the IEDB algorithm.

### Acknowledgments

We thank A. Sette and J. Sidney for providing advice on generating peptide pools, D. Hinz of LJI Flow cytometry core for sorting support, S. Liang for advice on scRNA-seq protocols, S. Rosales for assistance with sequencing, and J. Greenbaum of LJI Bioinformatics for MiXCR TCR sequence annotations. Mice were generated at the University of California San Diego Moores Cancer Center Transgenic Mouse Facility.

This work was funded in part by the National Institutes of Health (AI100663, Scripps Center for HIV/AIDS Vaccine Immunology and Immunogen Discovery, and AI144462, Scripps Consortium for HIV/AIDS Vaccine Development, to S. Crotty and W.R. Schief; R01 AI143826 to M.K. Jenkins) and the Collaboration for AIDS Vaccine Discovery (funding from the International AIDS Vaccine Initiative Neutralizing Antibody Center to W.R. Schief). The FACSaria II Cell Sorter was acquired through the National Institutes of Health Shared Instrumentation Grant Program (S10 RR027366).

**Author contributions:** The study was conceptualized by S. Crotty. J.H. Lee and S. Crotty designed experiments. J.H. Lee performed experimental work and analyzed data. J.K. Hu performed ELISPOT experiments. C. Nakao performed ELISAs and assisted in animal studies. G. Seumo and P. Vijayanand provided protocols and advice regarding scRNA-seq library preparation and performed sequencing. T. Dileepan and M.K. Jenkins generated MHC class II tetramers. E. Georgeson, B. Groschel, and W.R. Schief supplied immunogens. J.H. Lee and S. Crotty wrote the manuscript. All authors were asked to provide comments.

**Disclosures:** M.K. Jenkins reported a patent to US2019/044605 issued. W.R. Schief reported grants from Compuvax, Inc outside

the submitted work; in addition, W.R. Schief had a patent to BG505 GT3.1 pending and a patent to BG505 MD39 pending. No other disclosures were reported.

Submitted: 17 June 2020

Revised: 23 September 2020

Accepted: 13 November 2020

### References

- Abbott, R.K., and S. Crotty. 2020. Factors in B cell competition and immunodominance. *Immunol. Rev.* 296:120–131. <https://doi.org/10.1111/immr.12861>
- Abbott, R.K., J.H. Lee, S. Menis, P. Skog, M. Rossi, T. Ota, D.W. Kulp, D. Bhullar, O. Kalyuzhniy, C. Havenar-Daughton, et al. 2018. Precursor Frequency and Affinity Determine B Cell Competitive Fitness in Germinal Centers, Tested with Germline-Targeting HIV Vaccine Immunogens. *Immunity*. 48:133–146.e6. <https://doi.org/10.1016/j.immuni.2017.11.023>
- Angeletti, D., and J.W. Yewdell. 2018. Understanding and Manipulating Viral Immunity: Antibody Immunodominance Enters Center Stage. *Trends Immunol.* 39:549–561. <https://doi.org/10.1016/j.it.2018.04.008>
- Barnden, M.J., J. Allison, W.R. Heath, and F.R. Carbone. 1998. Defective TCR expression in transgenic mice constructed using cDNA-based alpha- and beta-chain genes under the control of heterologous regulatory elements. *Immunol. Cell Biol.* 76:34–40. <https://doi.org/10.1046/j.1440-1711.1998.00709.x>
- Baumjohann, D., S. Preite, A. Reboldi, F. Ronchi, K.M. Ansel, A. Lanzavecchia, and F. Sallusto. 2013. Persistent antigen and germinal center B cells sustain T follicular helper cell responses and phenotype. *Immunity*. 38:596–605. <https://doi.org/10.1016/j.immuni.2012.11.020>
- Behrens, A.-J., S. Vasiljevic, L.K. Pritchard, D.J. Harvey, R.S. Andev, S.A. Krumm, W.B. Struwe, A. Cupo, A. Kumar, N. Zitzmann, et al. 2016. Composition and Antigenic Effects of Individual Glycan Sites of a Trimeric HIV-1 Envelope Glycoprotein. *Cell Rep.* 14:2695–2706. <https://doi.org/10.1016/j.celrep.2016.02.058>
- Bianchi, M., H.L. Turner, B. Nogal, C.A. Cottrell, D. Oyen, M. Pauthner, R. Bastidas, R. Nedellec, L.E. McCoy, I.A. Wilson, et al. 2018. Electron-Microscopy-Based Epitope Mapping Defines Specificities of Polyclonal Antibodies Elicited during HIV-1 BG505 Envelope Trimer Immunization. *Immunity*. 49:288–300.e8. <https://doi.org/10.1016/j.immuni.2018.07.009>
- Bolotin, D.A., S. Poslavsky, I. Mitrophanov, M. Shugay, I.Z. Mamedov, E.V. Putintseva, and D.M. Chudakov. 2015. MiXCR: software for comprehensive adaptive immunity profiling. *Nat. Methods*. 12:380–381. <https://doi.org/10.1038/nmeth.3364>
- Briney, B., D. Sok, J.G. Jardine, D.W. Kulp, P. Skog, S. Menis, R. Jacak, O. Kalyuzhniy, N. de Val, F. Sesterhenn, et al. 2016. Tailored Immunogens Direct Affinity Maturation toward HIV Neutralizing Antibodies. *Cell*. 166:1459–1470.e11. <https://doi.org/10.1016/j.cell.2016.08.005>
- Brown, S.A., J. Stambas, X. Zhan, K.S. Slobod, C. Coleclough, A. Zirkel, S. Surman, S.W. White, P.C. Doherty, and J.L. Hurwitz. 2003. Clustering of Th cell epitopes on exposed regions of HIV envelope despite defects in antibody activity. *J. Immunol.* 171:4140–4148. <https://doi.org/10.4049/jimmunol.171.8.4140>
- Burton, D.R., and L. Hangartner. 2016. Broadly Neutralizing Antibodies to HIV and Their Role in Vaccine Design. *Annu. Rev. Immunol.* 34:635–659. <https://doi.org/10.1146/annurev-immunol-041015-055515>
- Burton, D.R., and J.R. Mascola. 2015. Antibody responses to envelope glycoproteins in HIV-1 infection. *Nat. Immunol.* 16:571–576. <https://doi.org/10.1038/ni.3158>
- Cao, L., J.K. Diedrich, D.W. Kulp, M. Pauthner, L. He, S.R. Park, D. Sok, C.Y. Su, C.M. Delahunty, S. Menis, et al. 2018. Global site-specific N-glycosylation analysis of HIV envelope glycoprotein. *Nat. Protoc.* 13:1196–1212. <https://doi.org/10.1038/nprot.2018.024>
- Cirelli, K.M., D.G. Carnathan, B. Nogal, J.T. Martin, O.L. Rodriguez, A.A. Upadhyay, C.A. Enemuo, E.H. Gebru, Y. Choe, F. Viviano, et al. 2019. Slow Delivery Immunization Enhances HIV Neutralizing Antibody and Germinal Center Responses via Modulation of Immunodominance. *Cell*. 177:1153–1171.e28. <https://doi.org/10.1016/j.cell.2019.04.012>
- Cottrell, C.A., J. van Schooten, C.A. Bowman, M. Yuan, D. Oyen, M. Shin, R. Morpurgo, P. van der Woude, M. van Breemen, J.L. Torres, et al. 2020.



- Mapping the immunogenic landscape of near-native HIV-1 envelope trimers in non-human primates. *PLoS Pathog.* 16:e1008753. <https://doi.org/10.1371/journal.ppat.1008753>
- Crooks, E.T., K. Osawa, T. Tong, S.L. Grimley, Y.D. Dai, R.G. Whalen, D.W. Kulp, S. Menis, W.R. Schief, and J.M. Binley. 2017. Effects of partially dismantling the CD4 binding site glycan fence of HIV-1 Envelope glycoprotein trimers on neutralizing antibody induction. *Virology*. 505: 193–209. <https://doi.org/10.1016/j.virol.2017.02.024>
- Crotty, S. 2019. T Follicular Helper Cell Biology: A Decade of Discovery and Diseases. *Immunity*. 50:1132–1148. <https://doi.org/10.1016/j.immuni.2019.04.011>
- Dan, J.M., C.S. Lindestam Arlehamn, D. Weiskopf, R. da Silva Antunes, C. Havenar-Daughton, S.M. Reiss, M. Brigger, M. Bothwell, A. Sette, and S. Crotty. 2016. A Cytokine-Independent Approach To Identify Antigen-Specific Human Germinal Center T Follicular Helper Cells and Rare Antigen-Specific CD4+ T Cells in Blood. *J. Immunol.* 197:983–993. <https://doi.org/10.4049/jimmunol.1600318>
- Deenick, E.K., A. Chan, C.S. Ma, D. Gatto, P.L. Schwartzberg, R. Brink, and S.G. Tangye. 2010. Follicular helper T cell differentiation requires continuous antigen presentation that is independent of unique B cell signaling. *Immunity*. 33:241–253. <https://doi.org/10.1016/j.immuni.2010.07.015>
- Depetris, R.S., J.-P. Julien, R. Khayat, J.H. Lee, R. Pejchal, U. Katpally, N. Cocco, M. Kachare, E. Massi, K.B. David, et al. 2012. Partial enzymatic deglycosylation preserves the structure of cleaved recombinant HIV-1 envelope glycoprotein trimers. *J. Biol. Chem.* 287:24239–24254. <https://doi.org/10.1074/jbc.M112.371898>
- Dhanda, S.K., S. Mahajan, S. Paul, Z. Yan, H. Kim, M.C. Jespersen, V. Jurtz, M. Andreatta, J.A. Greenbaum, P. Marcatili, et al. 2019. IEDB-AR: immune epitope database-analysis resource in 2019. *Nucleic Acids Res.* 47(W1): W502–W506. <https://doi.org/10.1093/nar/gkz452>
- Dosenovic, P., L. von Boehmer, A. Escolano, J. Jardine, N.T. Freund, A.D. Gitlin, A.T. McGuire, D.W. Kulp, T. Oliveira, L. Scharf, et al. 2015. Immunization for HIV-1 Broadly Neutralizing Antibodies in Human Ig Knockin Mice. *Cell*. 161:1505–1515. <https://doi.org/10.1016/j.cell.2015.06.003>
- Escolano, A., J.M. Steichen, P. Dosenovic, D.W. Kulp, J. Golijanin, D. Sok, N.T. Freund, A.D. Gitlin, T. Oliveira, T. Araki, et al. 2016. Sequential Immunization Elicits Broadly Neutralizing Anti-HIV-1 Antibodies in Ig Knockin Mice. *Cell*. 166:1445–1458.e12. <https://doi.org/10.1016/j.cell.2016.07.030>
- Finney, J., and G. Kelsoe. 2020. Ideal Vaccines: Balancing B Cell Recruitment and Differentiation. *Immunity*. 53:473–475. <https://doi.org/10.1016/j.immuni.2020.08.008>
- Go, E.P., G. Hewawasam, H.X. Liao, H. Chen, L.H. Ping, J.A. Anderson, D.C. Hua, B.F. Haynes, and H. Desaire. 2011. Characterization of glycosylation profiles of HIV-1 transmitted/founder envelopes by mass spectrometry. *J. Virol.* 85:8270–8284. <https://doi.org/10.1128/JVI.05053-11>
- Grundner, C., M. Pancera, J.-M. Kang, M. Koch, J. Sodroski, and R. Wyatt. 2004. Factors limiting the immunogenicity of HIV-1 gp120 envelope glycoproteins. *Virology*. 330:233–248. <https://doi.org/10.1016/j.virol.2004.08.037>
- Guttman, M., N.K. Garcia, A. Cupo, T. Matsui, J.-P. Julien, R.W. Sanders, I.A. Wilson, J.P. Moore, and K.K. Lee. 2014. CD4-induced activation in a soluble HIV-1 Env trimer. *Structure*. 22:974–984. <https://doi.org/10.1016/j.str.2014.05.001>
- Havenar-Daughton, C., D.G. Carnathan, A. Torrents de la Peña, M. Pauthner, B. Briney, S.M. Reiss, J.S. Wood, K. Kaushik, M.J. van Gils, S.L. Rosales, et al. 2016a. Direct Probing of Germinal Center Responses Reveals Immunological Features and Bottlenecks for Neutralizing Antibody Responses to HIV Env Trimer. *Cell Rep.* 17:2195–2209. <https://doi.org/10.1016/j.celrep.2016.10.085>
- Havenar-Daughton, C., J.H. Lee, and S. Crotty. 2017. Tfh cells and HIV bnAbs, an immunodominance model of the HIV neutralizing antibody generation problem. *Immunol. Rev.* 275:49–61. <https://doi.org/10.1111/imr.12512>
- Havenar-Daughton, C., S.M. Reiss, D.G. Carnathan, J.E. Wu, K. Kendrick, A. Torrents de la Peña, S.P. Kasturi, J.M. Dan, M. Bothwell, R.W. Sanders, et al. 2016b. Cytokine-Independent Detection of Antigen-Specific Germinal Center T Follicular Helper Cells in Immunized Nonhuman Primates Using a Live Cell Activation-Induced Marker Technique. *J. Immunol.* 197:994–1002. <https://doi.org/10.4049/jimmunol.1600320>
- Havenar-Daughton, C., A. Sarkar, D.W. Kulp, L. Toy, X. Hu, I. Deresa, O. Kalyuzhnyi, K. Kaushik, A.A. Upadhyay, S. Menis, et al. 2018. The human naive B cell repertoire contains distinct subclasses for a germline-targeting HIV-1 vaccine immunogen. *Sci. Transl. Med.* 10:eaat0381. <https://doi.org/10.1126/scitranslmed.aat0381>
- Hu, J.K., J.C. Crampton, A. Cupo, T. Ketas, M.J. van Gils, K. Sliepen, S.W. de Taeye, D. Sok, G. Ozorowski, I. Deresa, et al. 2015. Murine Antibody Responses to Cleaved Soluble HIV-1 Envelope Trimers Are Highly Restricted in Specificity. *J. Virol.* 89:10383–10398. <https://doi.org/10.1128/JVI.01653-15>
- Jardine, J., J.-P. Julien, S. Menis, T. Ota, O. Kalyuzhnyi, A. McGuire, D. Sok, P.-S. Huang, S. MacPherson, M. Jones, et al. 2013. Rational HIV immunogen design to target specific germline B cell receptors. *Science*. 340: 711–716. <https://doi.org/10.1126/science.1234150>
- Jardine, J.G., D.W. Kulp, C. Havenar-Daughton, A. Sarkar, B. Briney, D. Sok, F. Sesterhenn, J. Ereño-Orbea, O. Kalyuzhnyi, I. Deresa, et al. 2016. HIV-1 broadly neutralizing antibody precursor B cells revealed by germline-targeting immunogen. *Science*. 351:1458–1463. <https://doi.org/10.1126/science.aad9195>
- Kato, Y., R.K. Abbott, B.L. Freeman, S. Haupt, B. Groschel, M. Silva, S. Menis, D.J. Irvine, W.R. Schief, and S. Crotty. 2020. Multifaceted Effects of Antigen Valency on B Cell Response Composition and Differentiation In Vivo. *Immunity*. 53:548–563.e8. <https://doi.org/10.1016/j.immuni.2020.08.001>
- Keck, S., M. Schmalzer, S. Ganter, L. Wyss, S. Oberle, E.S. Huseby, D. Zehn, and C.G. King. 2014. Antigen affinity and antigen dose exert distinct influences on CD4 T-cell differentiation. *Proc. Natl. Acad. Sci. USA*. 111: 14852–14857. <https://doi.org/10.1073/pnas.1403271111>
- Klasse, P.J., T.J. Ketas, C.A. Cottrell, G. Ozorowski, G. Debnath, D. Camara, E. Francomano, P. Pugach, R.P. Ringe, C.C. LaBranche, et al. 2018. Epitopes for neutralizing antibodies induced by HIV-1 envelope glycoprotein BG505 SOSIP trimers in rabbits and macaques. *PLoS Pathog.* 14: e1006913–e1006920. <https://doi.org/10.1371/journal.ppat.1006913>
- Klasse, P.J., G. Ozorowski, R.W. Sanders, and J.P. Moore. 2020. Env Exceptionalism: Why Are HIV-1 Env Glycoproteins Atypical Immunogens? *Cell Host Microbe*. 27:507–518. <https://doi.org/10.1016/j.chom.2020.03.018>
- Locci, M., C. Havenar-Daughton, E. Landais, J. Wu, M.A. Kroenke, C.L. Arlehamn, L.F. Su, R. Cubas, M.M. Davis, A. Sette, et al. International AIDS Vaccine Initiative Protocol C Principal Investigators. 2013. Human circulating PD-1+CXCR3-CXCR5+ memory Tfh cells are highly functional and correlate with broadly neutralizing HIV antibody responses. *Immunity*. 39:758–769. <https://doi.org/10.1016/j.immuni.2013.08.031>
- McCoy, L.E., M.J. van Gils, G. Ozorowski, T. Messmer, B. Briney, J.E. Voss, D.W. Kulp, M.S. Macauley, D. Sok, M. Pauthner, et al. 2016. Holes in the Glycan Shield of the Native HIV Envelope Are a Target of Trimer-Elicited Neutralizing Antibodies. *Cell Rep.* 16:2327–2338. <https://doi.org/10.1016/j.celrep.2016.07.074>
- Mesin, L., J. Ersching, and G.D. Victora. 2016. Germinal Center B Cell Dynamics. *Immunity*. 45:471–482. <https://doi.org/10.1016/j.immuni.2016.09.001>
- Moody, M.A., I. Pedroza-Pacheco, N.A. Vandergrift, C. Chui, K.E. Lloyd, R. Parks, K.A. Soderberg, A.T. Ogbe, M.S. Cohen, H.-X. Liao, et al. 2016. Immune perturbations in HIV-1-infected individuals who make broadly neutralizing antibodies. *Sci. Immunol.* 1:aag0851. <https://doi.org/10.1126/sciimmunol.aag0851>
- Oseroff, C., J. Sidney, R. Vita, V. Tripple, D.M. McKinney, S. Southwood, T.M. Brodie, F. Sallusto, H. Grey, R. Alam, et al. 2012. T cell responses to known allergen proteins are differently polarized and account for a variable fraction of total response to allergen extracts. *J. Immunol.* 189: 1800–1811. <https://doi.org/10.4049/jimmunol.1200850>
- Oxenius, A., M.F. Bachmann, R.M. Zinkernagel, and H. Hengartner. 1998. Virus-specific MHC-class II-restricted TCR-transgenic mice: effects on humoral and cellular immune responses after viral infection. *Eur. J. Immunol.* 28:390–400. [https://doi.org/10.1002/\(SICI\)1521-4141\(199801\)28:01<390::AID-IMMU390>3.0.CO;2-O](https://doi.org/10.1002/(SICI)1521-4141(199801)28:01<390::AID-IMMU390>3.0.CO;2-O)
- Pabst, M., M. Chang, J. Stadlmann, and F. Altmann. 2012. Glycan profiles of the 27 N-glycosylation sites of the HIV envelope protein CN54gp140. *Biol. Chem.* 393:719–730. <https://doi.org/10.1515/hsz-2012-0148>
- Parker, R., T. Partridge, C. Wormald, R. Kawahara, V. Stalls, M. Aggelakopoulou, J. Parker, R.P. Doherty, Y.A. Morejon, E. Lee, et al. 2020. Mapping the SARS-CoV-2 spike glycoprotein-derived peptidome presented by HLA class II on dendritic cells. *bioRxiv*. <https://doi.org/10.1101/2020.08.19.255901> (Preprint posted August 20, 2020)
- Patil, V.S., A. Madrigal, B.J. Schmiedel, J. Clarke, P. O'Rourke, A.D. de Silva, E. Harris, B. Peters, G. Seumois, D. Weiskopf, et al. 2018. Precursors of human CD4+ cytotoxic T lymphocytes identified by single-cell transcriptome analysis. *Sci. Immunol.* 3:aan8664–14. <https://doi.org/10.1126/sciimmunol.aan8664>

- Pauthner, M., C. Havenar-Daughton, D. Sok, J.P. Nkolola, R. Bastidas, A.V. Boopathy, D.G. Carnathan, A. Chandrashekar, K.M. Cirelli, C.A. Cottrell, et al. 2017. Elicitation of Robust Tier 2 Neutralizing Antibody Responses in Nonhuman Primates by HIV Envelope Trimer Immunization Using Optimized Approaches. *Immunity*. 46:1073–1088.e6. <https://doi.org/10.1016/j.immuni.2017.05.007>
- Ranasinghe, S., M. Flanders, S. Cutler, D.Z. Soghoian, M. Ghebremichael, I. Davis, M. Lindqvist, F. Pereyra, B.D. Walker, D. Heckerman, and H. Streck. 2012. HIV-specific CD4 T cell responses to different viral proteins have discordant associations with viral load and clinical outcome. *J. Virol.* 86:277–283. <https://doi.org/10.1128/JVI.05577-11>
- Reiss, S., A.E. Baxter, K.M. Cirelli, J.M. Dan, A. Morou, A. Daigneault, N. Brassard, G. Silvestri, J.-P. Routy, C. Havenar-Daughton, et al. 2017. Comparative analysis of activation induced marker (AIM) assays for sensitive identification of antigen-specific CD4 T cells. *PLoS One*. 12: e0186998. <https://doi.org/10.1371/journal.pone.0186998>
- Ringe, R.P., P. Pugach, C.A. Cottrell, C.C. LaBranche, G.E. Seabright, T.J. Ketas, G. Ozorowski, S. Kumar, A. Schorcht, M.J. van Gils, et al. 2019. Closing and Opening Holes in the Glycan Shield of HIV-1 Envelope Glycoprotein SOSIP Trimers Can Redirect the Neutralizing Antibody Response to the Newly Unmasked Epitopes. *J. Virol.* 93:3–26. <https://doi.org/10.1128/JVI.01656-18>
- Sanders, R.W., R. Derking, A. Cupo, J.-P. Julien, A. Yasmeen, N. de Val, H.J. Kim, C. Blattner, A.T. de la Peña, J. Korzun, et al. 2013. A next-generation cleaved, soluble HIV-1 Env trimer, BG505 SOSIP.664 gp140, expresses multiple epitopes for broadly neutralizing but not non-neutralizing antibodies. *PLoS Pathog.* 9:e1003618. <https://doi.org/10.1371/journal.ppat.1003618>
- Sarkar, S., V. Kalia, M. Murphey-Corb, and R.C. Montelaro. 2002. Detailed analysis of CD4+ Th responses to envelope and Gag proteins of simian immunodeficiency virus reveals an exclusion of broadly reactive Th epitopes from the glycosylated regions of envelope. *J. Immunol.* 168: 4001–4011. <https://doi.org/10.4049/jimmunol.168.8.4001>
- Schwickert, T.A., G.D. Victora, D.R. Fooksman, A.O. Kamphorst, M.R. Mugnier, A.D. Gitlin, M.L. Dustin, and M.C. Nussenzweig. 2011. A dynamic T cell-limited checkpoint regulates affinity-dependent B cell entry into the germinal center. *J. Exp. Med.* 208:1243–1252. <https://doi.org/10.1084/jem.20102477>
- Seabright, G.E., K.J. Doores, D.R. Burton, and M. Crispin. 2019. Protein and Glycan Mimicry in HIV Vaccine Design. *J. Mol. Biol.* 431:2223–2247. <https://doi.org/10.1016/j.jmb.2019.04.016>
- Steichen, J.M., D.W. Kulp, T. Tokatlian, A. Escolano, P. Dosenovic, R.L. Stanfield, L.E. McCoy, G. Ozorowski, X. Hu, O. Kalyuzhnyi, et al. 2016. HIV Vaccine Design to Target Germline Precursors of Glycan-Dependent Broadly Neutralizing Antibodies. *Immunity*. 45:483–496. <https://doi.org/10.1016/j.immuni.2016.08.016>
- Steichen, J.M., Y.-C. Lin, C. Havenar-Daughton, S. Pecetta, G. Ozorowski, J.R. Willis, L. Toy, D. Sok, A. Liguori, S. Kratochvil, et al. 2019. A generalized HIV vaccine design strategy for priming of broadly neutralizing antibody responses. *Science*. 366:eaax4380. <https://doi.org/10.1126/science.aax4380>
- Stubbington, M.J.T., T. Lönnberg, V. Proserpio, S. Clare, A.O. Speak, G. Dougan, and S.A. Teichmann. 2016. T cell fate and clonality inference from single-cell transcriptomes. *Nat. Methods*. 13:329–332. <https://doi.org/10.1038/nmeth.3800>
- Sun, H.-X., Y. Xie, and Y.-P. Ye. 2009. ISCOMs and ISCOMATRIX. *Vaccine*. 27: 4388–4401. <https://doi.org/10.1016/j.vaccine.2009.05.032>
- Sun, L., D.R. Middleton, P.L. Wantuch, A. Ozdilek, and F.Y. Avci. 2016. Carbohydrates as T-cell antigens with implications in health and disease. *Glycobiology*. 26:1029–1040. <https://doi.org/10.1093/glycob/cww062>
- Sun, L., A.V. Paschall, D.R. Middleton, M. Ishihara, A. Ozdilek, P.L. Wantuch, J. Aceil, J.A. Duke, C.C. LaBranche, M. Tiemeyer, and F.Y. Avci. 2020. Glycopeptide epitope facilitates HIV-1 envelope specific humoral immune responses by eliciting T cell help. *Nat. Commun.* 11:2550. <https://doi.org/10.1038/s41467-020-16319-0>
- Surman, S., T.D. Lockey, K.S. Slobod, B. Jones, J.M. Riberdy, S.W. White, P.C. Doherty, and J.L. Hurwitz. 2001. Localization of CD4+ T cell epitope hotspots to exposed strands of HIV envelope glycoprotein suggests structural influences on antigen processing. *Proc. Natl. Acad. Sci. USA*. 98:4587–4592. <https://doi.org/10.1073/pnas.071063898>
- Tam, H.H., M.B. Melo, M. Kang, J.M. Pelet, V.M. Ruda, M.H. Foley, J.K. Hu, S. Kumari, J. Crampton, A.D. Baldeon, et al. 2016. Sustained antigen availability during germinal center initiation enhances antibody responses to vaccination. *Proc. Natl. Acad. Sci. USA*. 113:E6639–E6648. <https://doi.org/10.1073/pnas.1606050113>
- Tian, M., C. Cheng, X. Chen, H. Duan, H.-L. Cheng, M. Dao, Z. Sheng, M. Kimble, L. Wang, S. Lin, et al. 2016. Induction of HIV Neutralizing Antibody Lineages in Mice with Diverse Precursor Repertoires. *Cell*. 166:1471–1484.e18. <https://doi.org/10.1016/j.cell.2016.07.029>
- Tokatlian, T., B.J. Read, C.A. Jones, D.W. Kulp, S. Menis, J.Y.H. Chang, J.M. Steichen, S. Kumari, J.D. Allen, E.L. Dane, et al. 2019. Innate immune recognition of glycans targets HIV nanoparticle immunogens to germinal centers. *Science*. 363:649–654. <https://doi.org/10.1126/science.aat9120>
- Vita, R., S. Mahajan, J.A. Overton, S.K. Dhanda, S. Martini, J.R. Cantrell, D.K. Wheeler, A. Sette, and B. Peters. 2019. The Immune Epitope Database (IEDB): 2018 update. *Nucleic Acids Res.* 47(D1):D339–D343. <https://doi.org/10.1093/nar/gky1006>
- Wagh, K., E.F. Kreider, Y. Li, H.J. Barbican, G.H. Learn, E. Giorgi, P.T. Hraber, T.G. Decker, A.G. Smith, M.V. Gondim, et al. 2018. Completeness of HIV-1 Envelope Glycan Shield at Transmission Determines Neutralization Breadth. *Cell Rep.* 25:893–908.e7. <https://doi.org/10.1016/j.celrep.2018.09.087>
- West, A.P. Jr., R. Diskin, M.C. Nussenzweig, and P.J. Björkman. 2012. Structural basis for germ-line gene usage of a potent class of antibodies targeting the CD4-binding site of HIV-1 gp120. *Proc. Natl. Acad. Sci. USA*. 109:E2083–E2090. <https://doi.org/10.1073/pnas.1208984109>
- Williams, W.B., J. Zhang, C. Jiang, N.I. Nicely, D. Fera, K. Luo, M.A. Moody, H.-X. Liao, S.M. Alam, T.B. Kepler, et al. 2017. Initiation of HIV neutralizing B cell lineages with sequential envelope immunizations. *Nat. Commun.* 8:1732. <https://doi.org/10.1038/s41467-017-01336-3>
- Yamamoto, T., R.M. Lynch, R. Gautam, R. Matus-Nicodemus, S.D. Schmidt, K.L. Boswell, S. Darko, P. Wong, Z. Sheng, C. Petrovas, et al. 2015. Quality and quantity of TFH cells are critical for broad antibody development in SHIVAD8 infection. *Sci. Transl. Med.* 7:298ra120. <https://doi.org/10.1126/scitranslmed.aab3964>
- Yeh, C.-H., T. Nojima, M. Kuraoka, and G. Kelsoe. 2018. Germinal center entry not selection of B cells is controlled by peptide-MHCII complex density. *Nat. Commun.* 9:928. <https://doi.org/10.1038/s41467-018-03382-x>
- Zhumabekov, T., P. Corbella, M. Tolaini, and D. Kioussis. 1995. Improved version of a human CD2 minigene based vector for T cell-specific expression in transgenic mice. *J. Immunol. Methods*. 185:133–140. [https://doi.org/10.1016/0022-1759\(95\)00124-S](https://doi.org/10.1016/0022-1759(95)00124-S)

## Supplemental material

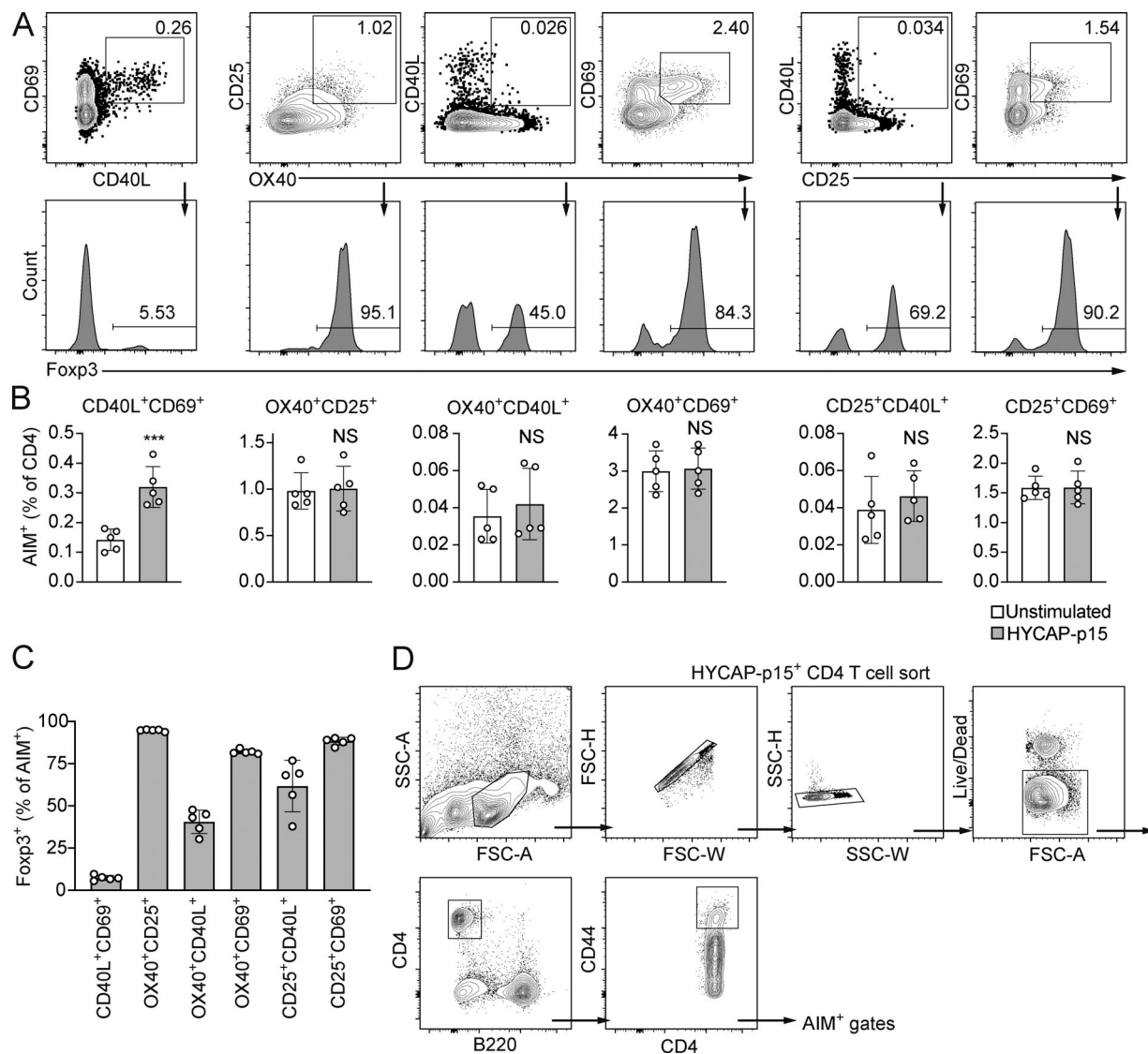
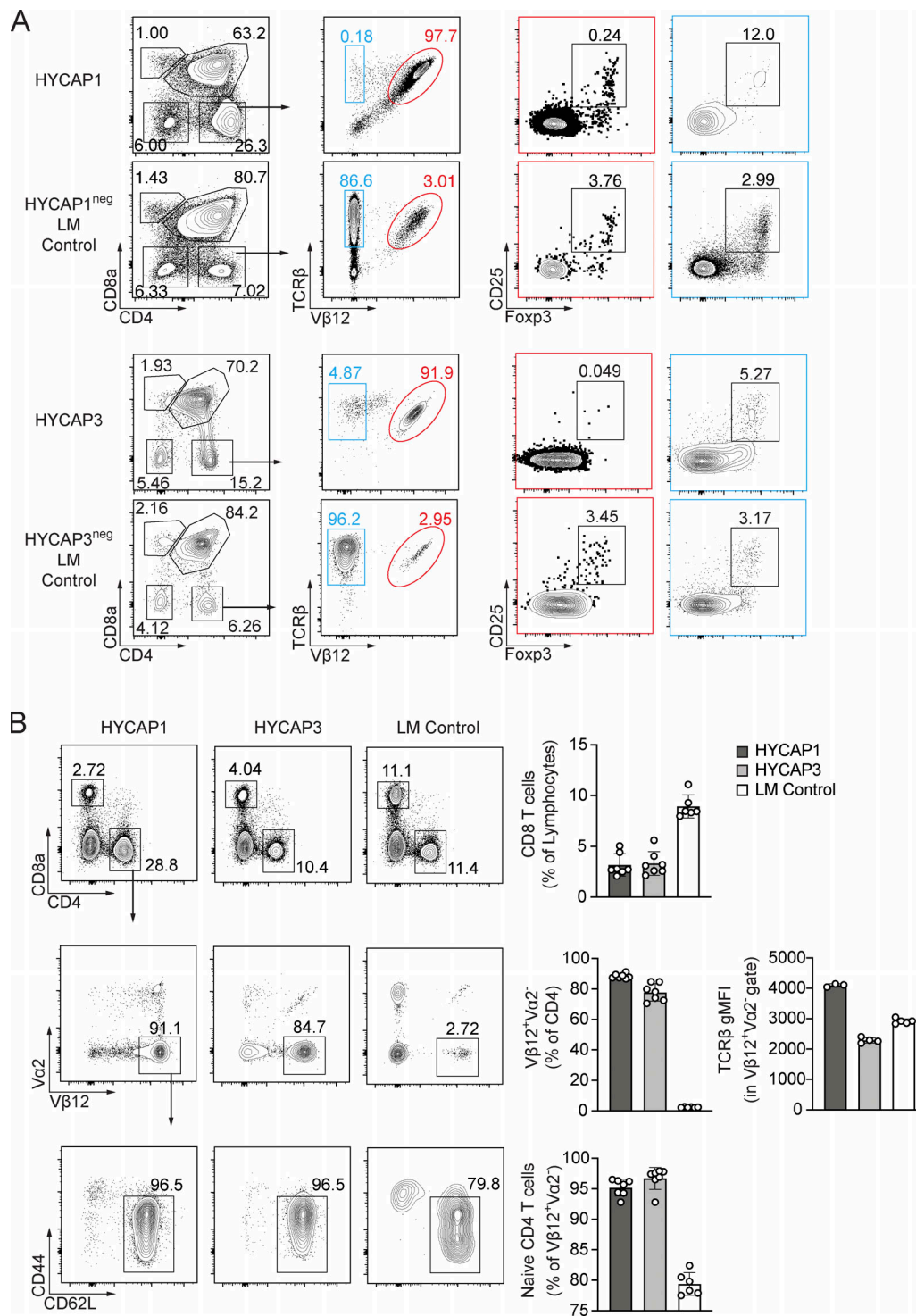
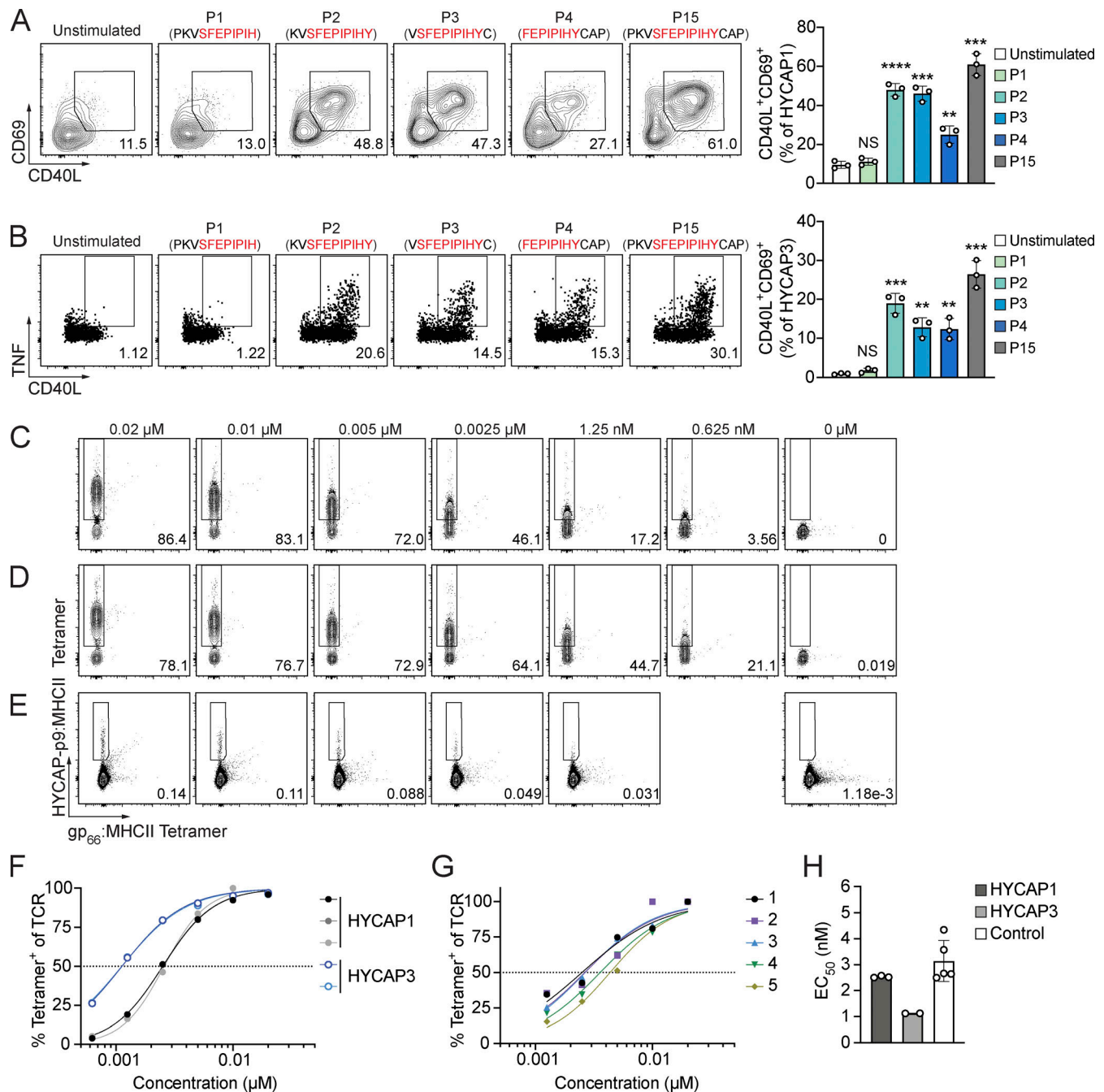


Figure S1. **Identification of antigen-specific CD4 T cells via antigen-induced surface markers. (A–C)** Surface markers tested for AIM assay for the detection of Ag-specific CD4 T cells in mice. Cells from BG505 SOSIP-immunized C57BL/6 mice were restimulated for 6 h with HYCAP-p15 peptide.  $N = 2$ ,  $n = 4–5$ , where  $N$  corresponds to number of independent experiments and  $n$  represents the number of mice per group in a given experiment. Representative data are shown. **(A)** Representative flow cytometry plots for HYCAP-p15-stimulated cells. AIM markers are gated on CD44<sup>+</sup>CD62L<sup>-</sup> activated CD4 T cells, and frequencies shown are percentages of AIM<sup>+</sup> CD4 T cells. **(B)** Quantification of HYCAP-p15-specific cells before and after stimulation by different AIM marker pairs. **(C)** Frequency of Foxp3<sup>+</sup> cells within the indicated AIM<sup>+</sup> gate. **(D)** Three mice were immunized i.p. with 20  $\mu$ g BG505 SOSIP trimer in alum, and spleens were harvested on day 8. Splenocytes were restimulated with 5  $\mu$ g/ml HYCAP-p15 peptide for 5 h and stained in preparation for sorting. Gating strategy used for sorting HYCAP-p15-specific T<sub>H</sub> and other combined T<sub>H</sub> subtypes. The final two gates within the CD44<sup>+</sup> population can be seen in Fig. 2 C.  $N = 1$ ,  $n = 3$ . Representative flow plot from one of the mice is shown. Mean and SD are graphed. NS, > 0.05; \*\*\*,  $P \leq 0.001$  (unpaired two-tailed Student's *t* test). FSC, forward scatter; SSC, side scatter.







**Figure S3. Estimation of relative affinities of HYCAP Tg TCRs.** (A and B)  $25 \times 10^3$  HYCAP1 or HYCAP3 CD4 T cells were adoptively transferred into congenically marked recipient mice (CD45.2 HYCAP1 into recipient CD45.1 C57BL/6 mice, and CD90.1 HYCAP3 into CD90.2 C57BL/6 mice) and then immunized with 20  $\mu$ g MD39-GT3.1 trimer. Mice were sacrificed 10 d after immunization, and cells were restimulated ex vivo for 5 h with the 15-mer peptide HYCAP-p15 or overlapping 11-mers derived from the HYCAP-p15 sequence. Fraction of HYCAP1 (A) or HYCAP3 (B) cells staining for antigen-specific markers after restimulation with the indicated peptides are shown. The flow plot shown is gated on CD4<sup>+</sup>/HYCAP<sup>+</sup> cells. The predicted core 9-mer epitope sequence is shown in red.  $N = 1$ ,  $n = 3$ , where  $N$  corresponds to number of independent experiments and  $n$  represents the number of mice per group in a given experiment. Statistics denote pairwise comparison between the unstimulated condition and each of the peptides. (C and D) Splenocytes from naive HYCAP1 (C) and HYCAP3 (D) mice were stained with the indicated concentrations of HYCAP-p9:MHCII tetramer (HYCAP-p9: SFEPIPIHY), along with a fixed concentration of an irrelevant LCMV gp<sub>66</sub>:MHCII tetramer. Gated on CD4 T cells.  $N = 1$ ,  $n = 2-3$ . (E) WT C57BL/6 mice were immunized with 20  $\mu$ g of MD39-GT3.1 Env trimer to proliferate Env-specific CD4 T cells. 7 d after immunization, total splenocytes were stained as in C and D. Gated on total CD4 T cells.  $N = 1$ ,  $n = 5$ . (F) Concentration of HYCAP-p9:MHCII tetramer used in staining plotted against proportion of total Tg HYCAP CD4 T cells bound to the tetramer. Maximum proportion of HYCAP Tg CD4 T cells in the mouse was defined by percentage of V $\beta$ 12<sup>+</sup>V $\alpha$ 2<sup>+</sup> CD4 T cells as shown in Fig. S2 B, stained as a separate panel to minimize interfering with the binding of tetramers. (G) As in F but plotted for polyclonal C57BL/6 HYCAP-p9-specific CD4 T cells shown in E. The maximum percentage of HYCAP-p9-specific polyclonal CD4 T cells was assumed to be the fraction of CD4 T cells binding to HYCAP-p9:MHCII at the highest concentration of the tetramer used for staining. (H) EC<sub>50</sub> defined by the concentration of tetramer required to obtain 50% of maximum TCR binding. Mean and SD are graphed. NS,  $P > 0.05$ ; \*\*,  $P \leq 0.01$ ; \*\*\*,  $P \leq 0.001$ ; \*\*\*\*,  $P \leq 0.0001$  (unpaired two-tailed Student's  $t$  test).

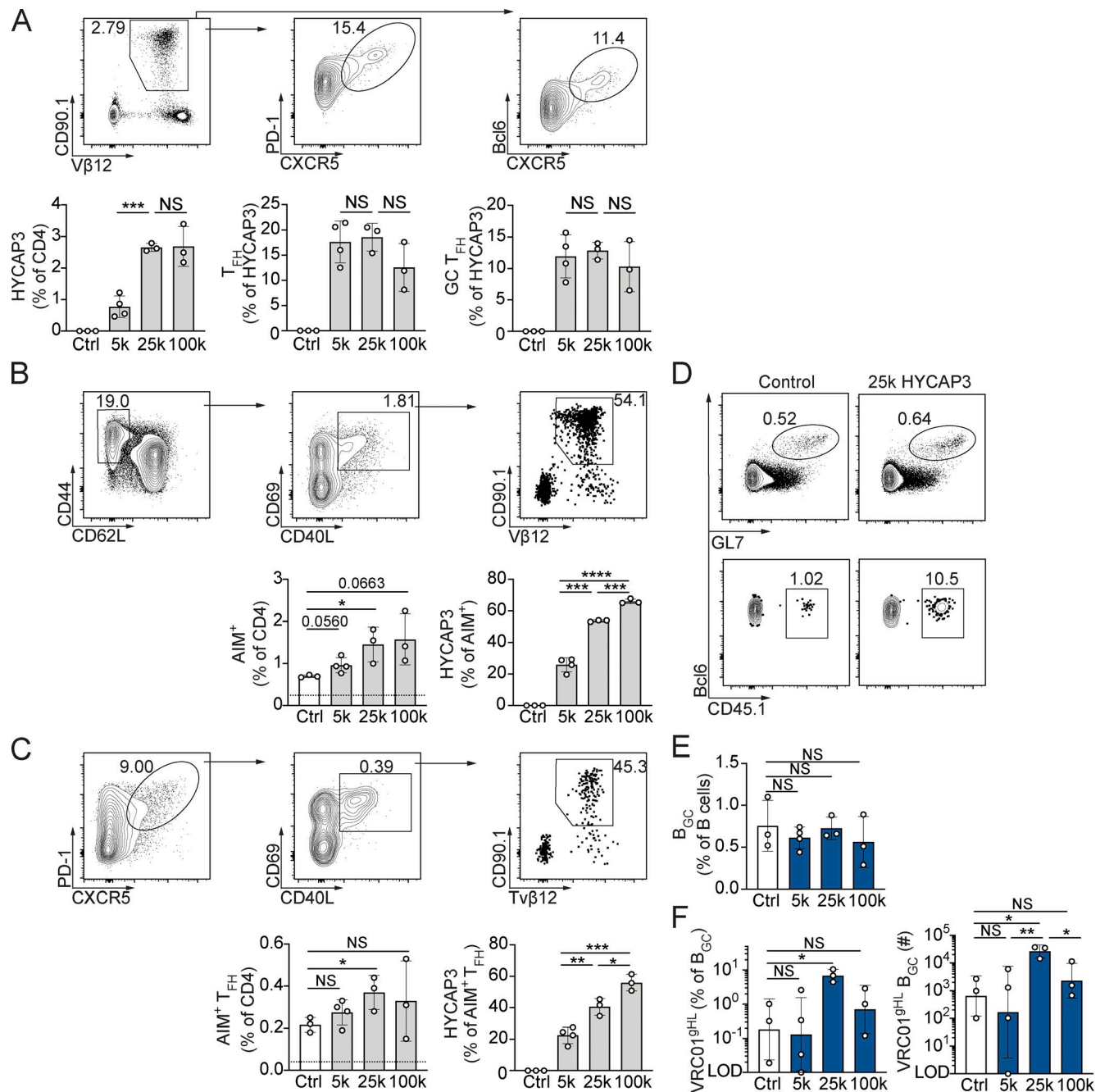


Figure S4. **B/T cell cotransfer model using HYCAP3 CD4 T cells.** (A–F) The indicated number of HYCAP3 CD4 T cells were cotransferred with  $10^3$  VRC01<sup>gH</sup> B cells and immunized i.p. with 20  $\mu$ g of MD39-GT3.1 trimer in alum.  $N = 3$ ,  $n = 3$ –4, where  $N$  corresponds to number of independent experiments and  $n$  represents the number of mice per group in a given experiment. Representative plots are shown. (A) Frequency of HYCAP3 CD4 T cells (CD90.1<sup>+</sup>Vβ12<sup>+</sup>) 10 d after immunization, and the proportion of HYCAP3 cells differentiated into T<sub>FH</sub> (PD-1<sup>+</sup>CXCR5<sup>+</sup>) or GC T<sub>FH</sub> (Bcl6<sup>+</sup>CXCR5<sup>+</sup>) cells. (B and C) Splenocytes were restimulated ex vivo for 5 h with BG505-MD39 MP. Representative flow plots are from the  $25 \times 10^3$  HYCAP3 transfer group. Frequencies shown in AIM gates are percent AIM<sup>+</sup> of CD4 T cells. (C) Total Env-specific CD4 T cells (CD4<sup>+</sup>/CD44<sup>+</sup>CD62L<sup>+</sup>/CD40L<sup>+</sup>CD69<sup>+</sup>) and proportion of HYCAP3 CD4 T cells within the AIM<sup>+</sup> gate (CD90.1<sup>+</sup>Vβ12<sup>+</sup>). (D) Env-specific T<sub>FH</sub> cells (CD4<sup>+</sup>/CD44<sup>+</sup>CD62L<sup>+</sup>/CXCR5<sup>+</sup>PD1<sup>+</sup>/CD40L<sup>+</sup>CD69<sup>+</sup>) and the fraction of those AIM<sup>+</sup> cells constituted by HYCAP3 cells (CD90.1<sup>+</sup>Vβ12<sup>+</sup>). (E) B<sub>GC</sub> cells (B220<sup>+</sup>/Bcl6<sup>+</sup>GL7<sup>+</sup>). (F) Frequency and number of VRC01<sup>gH</sup> B<sub>GC</sub> cells (CD45.1<sup>+</sup>CD45.2<sup>+</sup> within B<sub>GC</sub> cell gate). VRC01<sup>gH</sup> B<sub>GC</sub> cell number was back-calculated using the number of lymphocyte events collected and total number of lymphocytes counted from the spleen. Mean and SD are shown where data are plotted on a linear axis. Geometric mean and geometric SD are shown where data are plotted on a log axis. NS, > 0.05; \*,  $P \leq 0.05$ ; \*\*,  $P \leq 0.01$ ; \*\*\*,  $P \leq 0.001$ ; \*\*\*\*,  $P \leq 0.0001$  (unpaired two-tailed Student's  $t$  test).

Table S1 is provided online and lists the top-10th-percentile-ranked I-A<sub>b</sub> restricted epitopes in Env predicted by IEDB.